Cellular clearance and protein binding partners of pathogenic CEL-HYB

Renate Valdersnes Seierstad

This thesis is submitted in partial fulfilment of the requirements for the degree of Master in Biomedical Sciences.

Department of Biomedicine, Department of Clinical Medicine and Department of Clinical Science.

University of Bergen

Spring 2022

Table of Contents

Acknowledgements

I would like to thank my main supervisor, Karianne Fjeld, for willingly sharing your knowledge and experience, and for your support and guidance throughout the project. I am so grateful for having been welcomed and included in such exciting research. Your kindness and friendliness have inspired and motivated me. Whenever I had questions or challenges in the lab, your door has always been open – I immediately felt better after talking to you. Your inputs on my thesis have been priceless.

My sincere thanks also go to my co-supervisors Bente Berg Johansson and Anders Molven. Bente, thank you for your kind words, encouraging me to believe in myself and my work. I admire your scientific knowledge, and your feedback has been highly appreciated. Anders, I truly am inspired by your knowledge and enthusiasm. Thank you for your heart-warming care and always making sure I feel included in the CEL meetings and the group, and for your questions and feedback to make sure I always push myself just a bit further.

I also want to thank Ranveig Brekke Seim. You have been an important instructor for me in the lab in the most patient way. I have enormous respect for the way you take care of the mice, ensuring best possible animal welfare. Thank you for pleasant lunch breaks and checking in on me to make sure I'm fine. I would also like to thank Janniche Torsvik for your valuable suggestions and help with immunostaining. Thank you for very nice conversations and many laughs at the confocal microscope. Also, I would like to thank Solrun Steine for patiently helping me with Sanger sequencing, and answering all my questions, often the same questions several times. Thank you also to the rest of the Bergen CEL group for your discussions and input on my thesis; Khadija El Jellas, Jahedul Alam and Anny Gravdal Svanbring.

I am very grateful for all the help and support I received from Maria del Carmen Hernandez Valladares at PROBE, with the proteomics. Your help and guidance are greatly appreciated and have been very important for my thesis. I could not ask for better follow-up. I also want to thank Aishwarya Pavithram for helping me with cell culture and discussion about the proteomics.

Lastly, I would like to thank my husband, Kristofer. Thank you for encouraging me when I want to reach new goals, supporting me when the goals are hard to reach, and for loving me unconditionally.

Bergen, June 2022

Renate Valdersnes Seierstad.

Abbreviations

Selected abbreviations

ATG	Autophagy-related proteins
CEL/CEL	Carboxyl ester lipase gene/protein
CELP	Carboxyl ester lipase pseudogene
DM	Diabetes mellitus
ER	Endoplasmic reticulum
EV	Empty vector
HEK293 cells	Human embryonic kidney 293 cells
HYB	Hybrid
LC3B	Microtubule-associated protein 1A/1B-light chain 3 beta
LS-ESI-MS	Liquid Chromatography-Electrospray Ionization-Mass Spectrometry
MODY	Maturity onset diabetes of the young
NAHR	Non-allelic homologous recombination
PDAC	Pancreatic ductal adenocarcinoma
PPI	Protein-protein interaction
PTM	Post-translational modification
RT	Room temperature
T1D	Type 1 Diabetes
T2D	Type 2 Diabetes
TRUNC	Truncated artificial variant of CEL gene
UPS	Ubiquitin-proteasome system
VNTR	Variable number of tandem repeats
WT	Wild type

Abstract

The *CEL* gene encodes the digestive enzyme carboxyl ester lipase, which is mainly expressed in the acinar cells of the pancreas. In 2015, our research group discovered a *CEL* hybrid gene, named *CEL-HYB*, resulting from non-allelic homologous recombination between *CEL* and its pseudogene *CELP*. Interestingly, the *CEL-HYB* allele was found to be a genetic risk factor for chronic pancreatitis. In cellular studies performed by us and others, CEL-HYB showed reduced secretion, intracellular aggregation as well as induced cell stress and autophagy. Based on these findings, *CEL-HYB* allele is likely to belong to the misfolding-dependent pathway of genetic risk in chronic pancreatitis.

With this master's project, we wanted to study the cellular fate and to reveal potential protein binding partners of CEL-HYB, to learn more about its disease mechanism. To do so, we used both cellular and mouse model systems.

Our results showed that CEL-HYB is less secreted and tends to aggregate in the insoluble pellet fraction of transfected HEK293 cells. Moreover, Cel-HYB proteins accumulated on the inside of the apical cell membrane, forming a tubular-like expression pattern in the pancreatic acinar cells of mice. We also found the autophagy marker LC3B to be upregulated in the pancreas of Cel-HYB expressing mice, but not in control mice. By co-immunoprecipitation and mass spectrometry we discovered possible protein binding partners of CEL-HYB, including a cluster of nine proteins related to protein folding.

In summary, we have shown that CEL-HYB aggregation takes place both in the cell and at the organ level, strengthening the hypothesis that protein misfolding is involved in the disease mechanism. Misfolded CEL-HYB is then most likely cleared in the cell by induced autophagy. Interestingly, in our search for CEL-HYB binding partners we found proteins that facilitate the folding of other proteins. These results will be followed up and further analyzed in future studies.

1. Introduction

1.1 The pancreas

1.1.1 Anatomy and physiology of the human pancreas

The pancreas is a glandular organ located retroperitoneally and transversely in the upper abdomen (Figure 1.1). It lies between the duodenum and the spleen, just behind the stomach (1). In adult humans, the gland weighs about 80 g and is 14-18 cm long (2). It is surrounded by a fibrous capsule, which extends into the organ and divides the parenchyma into lobes and lobules (3). The organ is anatomically divided into four parts, namely the head, neck, body, and tail (Figure 1.1). The head is located next to the duodenum, while the tail is located next to the splenic hilum (4). The common bile duct passes through the head of the pancreas and joins with the pancreatic duct when entering the duodenum. The pancreas gets its blood supply from the celiac and the superior mesenteric arteries, while the venous drainage goes through the splenic and superior mesenteric vein, into the portal vein. Both the sympathetic and parasympathetic nervous system innervate the pancreas (2).

The pancreas is the only organ with both exocrine and endocrine functions. As described in more details below, the endocrine cells secrete hormones regulating glucose homeostasis, whereas the exocrine pancreas produces digestive enzymes and bicarbonate.

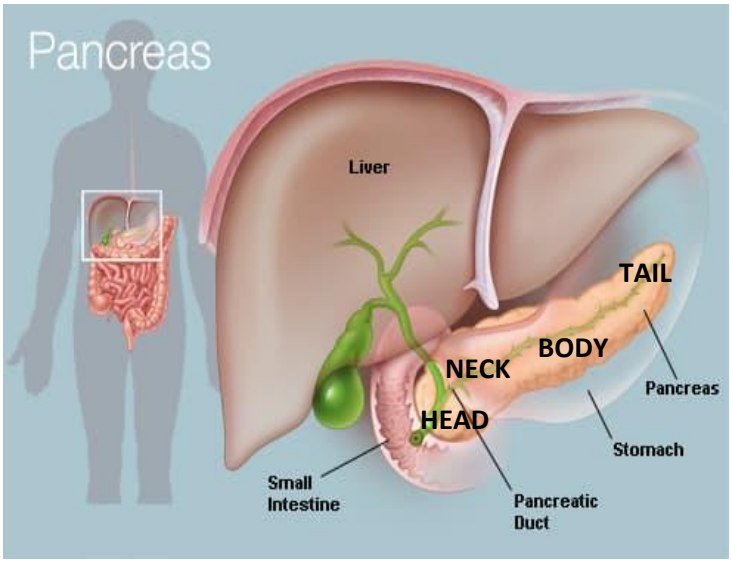

Figure 1.1. Anatomical overview and relations of the pancreas. The pancreas is located in the upper abdomen, just below the liver. It has four anatomical units: the head, neck, body, and tail. The pancreatic duct joins with the common bile duct in the head of the pancreas, before entering the duodenum. Modified from ©2016, WebMD, LLC. All rights reserved.

1.1.2 The endocrine pancreas

The endocrine pancreas makes up about 2-4 % of the total pancreas volume. It is organized into small clusters of cells named islets of Langerhans, which are diffusely spread throughout the organ (Figure 1.2). Some studies have reported a continuous increase in density of islets from the pancreatic head to the tail (increasing from 2 to 4 %) (3, 5). The islets vary in size and can include only a few to several thousand endocrine cells. Single endocrine cells can also be found spread throughout the acinar and ductal tissue (6).

In the islets, there are at least 5 different hormone-secreting cells. The insulin-producing beta cells make up about 50-70 % of the endocrine organ. The alpha cells comprise 20-40 % and produce and secrete glucagon. The main function of the endocrine pancreas is tight regulation of glucose homeostasis, mainly by the hormones insulin and glucagon (7). In addition to the dominating alpha and beta cells, there are other cells which add up to a few percentages of the islet cell types. Delta cells secrete somatostatin which blocks the secretion of both insulin and glucagon from adjacent cells (Figure 1.2) (8). PP cells secrete pancreatic polypeptide (PP) that inhibits pancreatic secretion of bicarbonate, enzymes, and fluid (9). Finally, epsilon cells release the hormone ghrelin, which modulates insulin release, and is involved in the regulation of food intake, inflammation, and energy expenditure (3, 10). In the human pancreas, the endocrine cells are randomly distributed throughout the islet (Figure 1.2) (11).

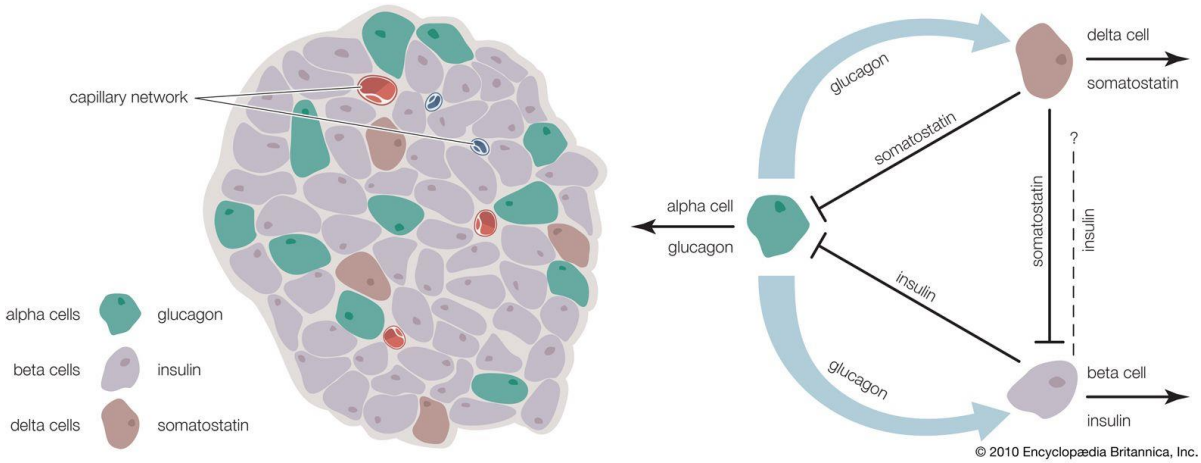

Figure 1.2 Endocrine cells in the islet of Langerhans. The three most common cell types in the islets are alpha, beta and delta cells secreting glucagon, insulin, and somatostatin, respectively. This figure illustrates the random spread of the different cell types and their abundance. The hormones produced have an effect on the neighboring cells; insulin inhibits alpha cells, glucagon stimulates delta and beta cells, and somatostatin inhibits both alpha and beta cells. *Reproduced from reference (12).*

1.1.3 The exocrine pancreas

The exocrine pancreas accounts for 96-99 % of the total pancreas volume (13). It is organized into lobes, which in turn are made up of smaller lobules. Each lobule is composed of several acini (Figure 1.3). An acinus is a cluster of pyramidal acinar cells with a lumen in the middle. The acinus is the functional unit of the exocrine pancreas. Acinar cells are responsible for producing, storing, and secreting digestive enzymes (3). They are polarized cells with the apical side towards the lumen. The nucleus and endoplasmic reticulum (ER) are located in the basal region, whereas the zymogen granules, containing the digestive enzymes, are stored in the apical region (14). The stored digestive enzymes are released from the zymogen granules and secreted out of the acinar cells by exocytosis. The secretion is mainly stimulated by the hormones gastrin, cholecystokinin (CKK) and secretin (2). As illustrated in Figure 1.3, the duct system consists of centroacinar cells and duct epithelial cells which secrete bicarbonate, water, Na^+ and K^+ (13, 15). The centroacinar cells are cuboidal-shaped and positioned at the junction between the acinus and the ductal cells which form the ductal lining (5).

There are four main types of digestive enzymes secreted from the pancreas; proteases, amylases, lipases and nucleases – digesting proteins, carbohydrates, fat and DNA/RNA respectively (Table 1) (16). These digestive enzymes together with water, bicarbonate, Na^+ and K^+, make up the pancreatic juice. The pancreatic juice is secreted into small intercalating ducts, which drain into larger intralobular ducts (Figure 1.3). Several intralobular ducts converge into one main pancreatic duct which joins the common bile duct before entering the duodenum through the major duodenal papilla (ampulla of Vater) (17).

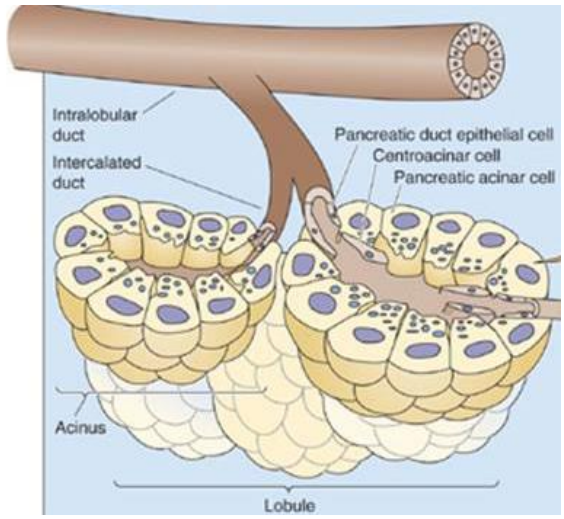

Figure 1.3 Structure of the exocrine pancreas. The exocrine pancreas is made up of functional units, called acini, which surround intercalated ducts. The acinar cells secrete digestive enzymes into the ducts. Centroacinar cells secrete bicarbonate, Na^+ and K^+ and are located at the junction between the acinus and the ductal cells. The intercalated ducts merge to intralobular ducts *Reproduced from reference (18)*.

Table 1 Main types of pancreatic digestive enzymes

Digestive enzyme category	Secreted as	Examples
Protease	Proenzymes	Trypsinogen (converted into trypsin)
Amylase	Active enzymes	α-amylase
Lipase	Active enzymes	Carboxyl ester lipase
Nuclease	Active enzymes	RNase A

Pancreatic secretion can be divided into 3 phases: the cephalic, gastric, and intestinal phase. The cephalic phase (before the food is swallowed) and the gastric phase (when the food is in the stomach) stimulate pancreatic enzyme secretion at up to 50 % of maximal secretory rate, but with no increase in bicarbonate secretions (19). In the intestinal phase (when the digested food enters the duodenum) high concentrations of bicarbonate are secreted. Because of this high concentration of bicarbonate, the pancreatic juice is alkaline and therefore neutralizes the gastric acid during enzymatic digestion of nutrients (20).

Zymogen granules take up about 30 % of the total acinar cell volume (21). From the acini the digestive enzymes are released into the lumen of intercalating ducts (Figure 1.3) through exocytosis (2). Functional receptors mediating the release of digestive enzymes have been identified for CCK, acetylcholine, gastrin-releasing peptide (GRP), substance P, vasoactive intestinal peptide (VIP) and secretin. These receptors are G-protein-coupled-receptors (GPCRs) on the basolateral plasma membrane of the acinar cells (22). VIP and secretin function through adenylate cyclase and increased cellular cAMP, which leads to enzyme secretion via cAMP-dependent protein kinase A, while CCK and acetylcholine function through the phosphoinositide-calcium signaling system. Phospholipase C mediates hydrolysis of phosphatidylinositol 4,5-bisphopshate to 1,2 diacylglycerol and inositol 1,4,5-trisphosphate (IP_3). IP_3 releases calcium from the ER into the cytosol which leads to secretion of digestive enzymes. There is extensive crosstalk between these two cascades (2, 21).

1.2 Disease of the endocrine pancreas

1.2.1 Diabetes mellitus

Diabetes mellitus (DM) is a metabolic disease characterized by an aberration of glucose homeostasis that causes chronic hyperglycemia. It is estimated that 260 000 – 280 000 people have diagnosed DM in Norway per 2020 (23). DM results from defective insulin synthesis, secretion and/or action (24). Initial symptoms include polyuria, polydipsia, weight loss,

polyphagia, and blurred vision. The long-term effects can be damage, dysfunction and failure of organs like eyes, kidneys, nerves, heart and blood vessels (25). There are different types of DM, the two most common ones being type 1 and type 2. Other types include monogenic, gestational, latent autoimmune diabetes in adults, and a few more.

Type 1 Diabetes mellitus (T1D) makes up about 5-10 % of the cases and is caused by an absolute deficiency in insulin secretion due to autoimmune destruction of the pancreatic beta cells. One or more types of autoantibodies are often present at the time when fasting hyperglycemia is first detected. The rate of destruction of beta cells varies. T1D most often presents in childhood and adolescence, but can occur at any age (25).

A serious and life-threatening complication to diabetes (particularly type 1 diabetes) is diabetic ketoacidosis (DKA). Because of absolute insulin deficiency, gluconeogenesis and glycogenolysis is accelerated, and there is decreased glucose utilization. This leads to increased lipolysis and decreased lipogenesis. The free fatty acids are turned into ketone bodies (beta-hydroxybutyrate, acetoacetate and acetone). Patients with DKA therefore often present with metabolic acidosis, hyperglycemia, and hyperketonemia.

Type 2 Diabetes mellitus (T2D) makes up about 90-95 % of the diabetes cases. These patients have insulin resistance and a relative insulin deficiency, as opposed to the absolute deficiency in T1D. Therefore, T2D patients often do not need insulin, and autoimmune destruction of β-cells does not occur. Risk factors are age, obesity, and lack of physical activity. T2D often has a strong genetic predisposition, but the genetics are complex and not fully defined (25). Long-term effects are micro- and macrovascular complications.

Monogenic diabetes. There are two main forms of monogenic diabetes: neonatal diabetes mellitus which occurs in newborns and infants, and maturity-onset diabetes of the young (MODY), which occurs in adolescents and young adults (26). There are more than 20 known genetic causes for neonatal diabetes mellitus, and it is categorized as either transient, permanent, or syndromic form. The symptoms often present within 6 months of age (27). Patients with MODY are often wrongly diagnosed as either T1D or T2D and may explain 1-5 % of all diabetes cases (28). MODY usually presents before the age of 25 and is characterized by progressive β-cell dysfunction. The disease has an autosomal dominant hereditary pattern. It is distinguished from T1D by measurable C-peptide (a short chain of amino acids produced as a byproduct when producing insulin) and absence of autoantibodies, and it does not lead to DKA (28). Mutations in at least 11 different genes can lead to MODY (29).

1.3 Diseases of the exocrine pancreas

1.3.1 Acute Pancreatitis

Acute pancreatitis is an inflammatory disease of the pancreas. In Norway, 13 - 45 per 100.000 people develop the disease each year (30). The criteria for diagnosing acute pancreatitis are abdominal pain, serum lipase (or amylase) at least three times the normal level, and findings on diagnostic imaging (CT, MRI or ultrasound) (31). Well-known risk factors are alcohol abuse and gallstones. However, only 2 % of patients with asymptomatic gallstones, and 2 - 3 % of heavy drinkers develop pancreatitis. It is therefore likely that genetic and other risk factors are involved (31). For example, smoking has been suggested to be a risk factor for acute pancreatitis with a dose-response relationship (32) and four retrospective studies show increased risk of acute pancreatitis in T2D, especially in younger patients (31). The mechanism behind acute pancreatitis relates to pancreatic duct obstruction, which leads to upstream blockage of pancreatic secretion. The zymogen granules accumulate and fuse with lysosomes, implying that lysosomal enzymes can convert trypsinogen into trypsin. This leads to the accumulation of active trypsin inside the cell followed by autodigestive injury. Zymogen granules are released from the basolateral membrane of the acinar cells, into the interstitial tissue, leading to protease-induced injury (31). This injury stimulates an inflammatory response in the pancreas. However, studies have shown that inflammatory infiltration also can occur without trypsinogen-activation, like dysfunctional calcium signaling, impaired autophagy, ER stress, the unfolded protein response or mitochondrial dysfunction (33). Acute pancreatitis can range from mild to severe and may in worst case end in sepsis, multiorgan failure and even death.

1.3.2 Chronic Pancreatitis

Chronic pancreatitis is a multifactorial, fibroinflammatory syndrome of the exocrine pancreas (34). In Norway, 1 - 10 per 100.000 people develop the disease each year (35). It is characterized by pancreatic atrophy, fibrosis, ductal structures and distortion, calcifications, dysplasia, exocrine insufficiency, diabetes and chronic pain (36). The most prevalent risk factors are alcohol and tobacco, but they seldom lead to chronic pancreatitis alone (34). Other risk factors are pancreatic duct obstruction, hypertriglyceridemia, chronic kidney disease, IgG4-related disease (autoimmune pancreatitis type 1) and genetic mutations. Some of the known mutations that increase the risk of chronic pancreatitis are found in the genes serine peptidase inhibitor kazal type 1 (*SPINK1),* chymotrypsin C *(CTRC),* chymotrypsinogen B1-chymotrypsinogen B2 (*CTRB1-CTRB2),* cystic fibrosis transmembrane conductance regulator (*CFTR),* claudin 2

(*CLDN2)* or MORC family CW-type zinc finger protein 4 (*MORC4)* and carboxyl ester lipase *(CEL)* (34).

It is a widely accepted model that chronic pancreatitis starts with as an acute event which causes significant acinar cell stress or injury resulting in clinical acute pancreatitis. The patients are thereafter susceptible to recurrent episodes of acute pancreatitis, which leads to recurrent injury of the acinar cells and chronic inflammation, resulting in fibrosis (36). Some patients, however, do not suffer any episodes of clinical acute pancreatitis, and are assumed to have subclinical episodes leading to chronic pancreatitis (36). Another theory is the obstructive hypothesis where a protein-plug is formed due to hypersecretion and protein precipitation. This plug then calcifies and obstructs the pancreatic ducts (36). The reason for abdominal pain in chronic pancreatitis is poorly understood and may come from episodic acute pancreatitis, ductal obstruction leading to ductal hypertension, structural complications like inflammatory head mass, pseudocyst, or pancreatic cancer. However, often inflammation or structural complications are not seen in patients with chronic pain, and the reason may therefore be neuropathic pain (36).

1.3.3 Hereditary Pancreatitis

Hereditary pancreatitis is associated with mutations in the cationic trypsinogen gene (*PRSS1*). Approximately 1 % of patients with chronic pancreatitis have hereditary pancreatitis (37). This disorder has an autosomal dominant inheritance pattern with high penetrance. It has an early onset at about 30 years of age and a slower progression than other forms of chronic pancreatitis (37, 38). Most patients have mild symptoms, but the clinical presentation is highly variable. Symptoms may include chronic abdominal pain, decreased endocrine and exocrine pancreatic function, nausea, and vomiting, maldigestion, diabetes, pseudocysts, bile duct and duodenal obstruction and pancreatic cancer (38). Patients with hereditary pancreatitis have an accumulated life time risk of 20 - 50 % chance of developing pancreatic cancer, due to the early presentation of the disease (37). Some of the *PRSS1* mutations lead to increased autocatalytic conversion of trypsinogen to active trypsin while still in the pancreas. Other mutations prevent trypsin from being broken down (39).

1.3.4 Pancreatic Cancer

Pancreatic cancer is a highly invasive malignant tumor with a high fatal risk. In Norway, pancreatic cancer causes 5 % of all cancer related deaths, and is diagnosed in about 900 people per year (40). It makes up 2 % of all cancers worldwide (41). There are few and unspecific symptoms, which means that the cancer often has progressed when detected. Risk factors for

pancreatic cancer is smoking, chronic pancreatitis, family history of pancreatic cancer, high age (>60 years), male gender and obesity (42). Other studies have found factors like alcohol, abnormal metabolism of microorganisms, blood type and glucose and lipase levels to influence the risk (41). Inherited mutations in cancer genes can also lead to pancreatic cancer (41).

Pancreatic ductal adenocarcinoma (PDAC) is the most common type of pancreatic cancer. This cancer develops from non-invasive precursor lesions like pancreatic intraepithelial neoplasia, or from intraductal papillary mucinous neoplasms or mucinous cystic neoplasms (42). The most frequent genetic abnormalities associated with PDAC at the somatic (acquired) level is mutations in the *K RAS* oncogene, or in tumor suppressor genes like *CDKN2A*, *TP53* and *SMAD4* (42). Microbial dysbiosis in different parts of the body also is found to be associated with susceptibility, occurrence, and prognosis of PDAC. An example of this is periodontitis, where the bacteria *Corynebacterium* and lectins increase the risk of PDAC (41).

1.4 Carboxyl Ester Lipase (CEL)

1.4.1 The human *CEL* gene

The human *CEL* gene is located on chromosome number 9, q34.13, and spans a region of approximately 10 kilobases (kb). *CEL* is a well conserved protein-coding gene, consisting of 11 exons interrupted by 10 introns (Figure 1.4) (43). Exon 11 consists of a variable number of tandem repeat (VNTR) region. Each repeat consists of nearly identical 33 base pair segments. In humans, the number of VNTR repeats vary from 3-23, the most common being 16 (44, 45). A *CEL* pseudogene (*CELP*) is localized 11 kb downstream of *CEL*. This gene covers about 5 kb, and lacks exon 2-7 compared to *CEL* (Figure 1.4) (43). *CEL* is not expected to translate into a functional protein (43, 46). Actually, it seems that *CEL* is a newly duplicated gene that has become active, while the original gene was *CELP*, and has later been inactivated (47).

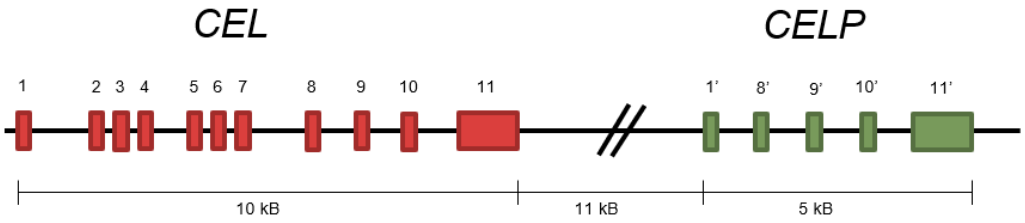

Figure 1.4 Structure of the human carboxyl ester lipase locus. The human *CEL* gene (red) consists of 11 exons. A *CEL* pseudogene (*CEL-P*) (green) is localized 11 kb downstream and lacks exon 2-7 compared to *CEL*. Adapted from *Fjeld et.al.* 2015. *Nat.Genet.*

1.4.2 The CEL protein

The *CEL* gene encodes carboxyl ester lipase, a digestive enzyme found in all vertebrates examined to date (48). The CEL protein is mainly secreted from the acinar cells of the exocrine pancreas into the duodenum and makes up about 4 % of the pancreatic juice (45). CEL was previously known as bile salt-stimulated (or dependent) lipase (BSSL or BSDL) since most of its actions are stimulated by bile salt in the duodenum (49). CEL is a glycoprotein with a relatively high carbohydrate content (9%) (50). The enzyme hydrolyzes dietary fat, fat-soluble vitamins, cholesteryl esters and branched fatty acid esters of hydroxyl fatty acids (45, 49). CEL is also produced in lactating mammary glands and secreted with the breast milk to aid the breast-fed infant's endogenous capacity for intestinal fat digestion (51).

The structure of CEL protein is shown in Figure 1.5. The globular domain includes an N-terminal signaling peptide, bile salt binding sites and catalytic sites (49). The signaling peptide functions to translocate the protein from the cytoplasm to ER. The catalytic activity of CEL consists of the triad Ser-194, His-435 and Asp 320, and forms a site for substrate hydrolysis. The C-terminal end of the protein includes the VNTR domain (52). The repeats are made up of 11 amino acids encoded by the nearly identical 33 base pair-segments in the VNTR region of the *CEL* gene. The sequence is enriched in proline (P), glutamine (E), serine (S) and threonine (T) (so-called PEST sequence). The molecular weight of the CEL protein varies due to the varying number of repeats. The most common human CEL variant containing 16 VNTR repeats consists of 722 amino acids and has a theoretical molecular mass of 79 kDa (Figure 1.5) (45).

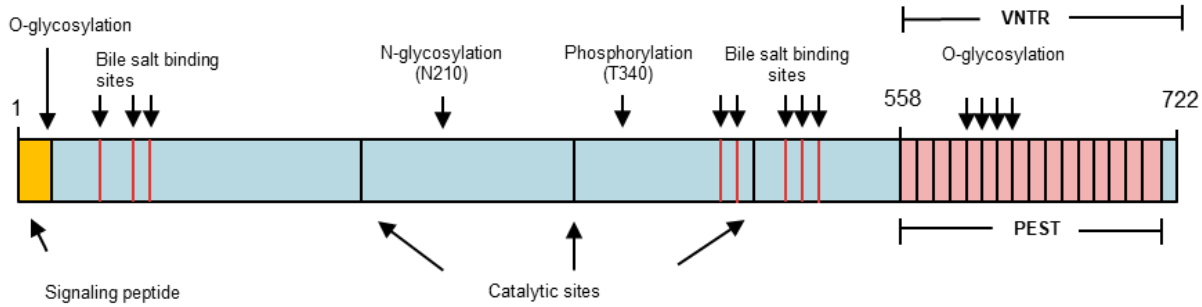

Figure 1.5 Structure of the human carboxyl ester lipase protein. CEL has an N-terminal signaling peptide (yellow), bile salt binding sites (red) and catalytic sites. It is heavily O-glycosylated. The enzyme has a C-terminal end that includes the VNTR domain (pink). The VNTR repeats are made up of 11 amino acids encoded by the nearly identical 33 base pair-segments. The VNTR domain encodes a PEST sequence. Adapted from *Fjeld et.al.* 2015. *Nat.Genet.*

CEL is secreted through the secretory pathway, and travels from the ER to the Golgi apparatus before being secreted. The pathway starts already while the protein is being translated on ribosomes. The protein enters the ER co-translationally, where it folds together with several chaperones (53). CEL is N-glycosylated at Asn187, which is important for folding and secretion. Then it is transported to the Golgi where it is heavily O-glycosylated in the VNTR region. The CEL protein has 36 potential sites for O-glycosylation (54, 55). The VNTR domain encodes a PEST sequence (rich in proline, glutamic acid, serine and threonine), which can be a signal for rapid protein degradation. This PEST sequence may be masked by the O-glycosylation, increasing CEL's stability (Figure 1.5) (56). The glycosylation may also reduce proteolytic degradation in the duodenum and could be important for the solubility of the protein (57). Finally, CEL is phosphorylated at residue Thr340 in the *trans*-Golgi network. This allows translocation through the secretory pathway, and co-storage in zymogen granules together with other digestive enzymes (58).

1.5 Carboxyl Ester Lipase in Human Disease

1.5.1 MODY 8

As mentioned above, MODY is a monogenic form of diabetes with an autosomal dominant inheritance. MODY8 was reported for the first time in 2006 by our research group (44). MODY8 not only leads to diabetes, but also to a slowly progressing pancreatic exocrine dysfunction with fatty replacement of pancreatic parenchyma (lipomatosis) and development of pancreatic cysts (45). The MODY8 patients present in their early twenties with mild to moderate abdominal pain and exocrine pancreatic dysfunction, but not necessarily any clinical signs of chronic pancreatitis. The causative mutation in the first MODY8 family was a single-bp deletion in the first repeat of the CEL VNTR. The second MODY8 family had a single-bp deletion in VNTR repeat 4. Besides the two Norwegian families three other families with MODY8 have been discovered: one from Sweden (59), one from the Czech Republic (59) and one Italian family (60). Based on current knowledge, the disease mechanisms are linked to ER stress, apoptosis, and protein aggregation with activation of the unfolded protein response (55, 61). Recently, it was shown how the MODY8 mutation of *CEL* may promote endocrine dysfunction by being taken up in beta-cells and negatively influencing their function (62).

1.5.2 Chronic Pancreatitis

In 2015, our research group identified a new pathogenic variant of the *CEL* gene, namely *CEL-HYB*. This variant was found to be a genetic risk factor for chronic pancreatitis, as the *CEL-HYB* allele was overrepresented by five-fold in cases compared to healthy controls (63). In three independent Asian cohorts studied, *CEL-HYB* was not found, suggesting that it is an ethnic-specific risk allele (64). However, they did find an alternative *CEL-HYB* allele, and named it *CEL-HYB*2. *CEL-HYB* detected in 2015 was then renamed to *CEL-HYB1*. In this thesis I will refer to *CEL-HYB1* as *CEL-HYB.*

CEL-HYB is likely a result of non-allelic homologous recombination (NAHR), with the crossover occurring in intron 10 of *CEL* and its neighboring pseudogene *CELP* (Figure 1.6). NAHR usually occurs when there are high sequence similarities between two genes. *CEL* and *CELP* have 97 % sequence similarity.

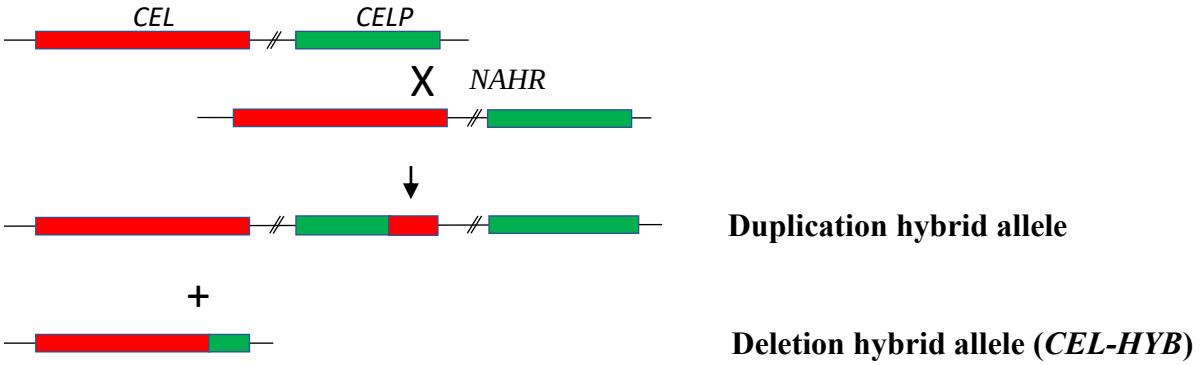

Figure 1.6 Non-allelic homologous recombination (NAHR) between *CEL* and *CELP*. Probable mechanism of how *CEL-HYB* (deletion hybrid allele) originated by non-allelic homologous recombination between *CEL* and *CELP*. The duplication hybrid allele is unlikely to encode a functional protein due to a premature stop codon in *CEL*P exon 8. However, the deletion hybrid allele, i.e., *CEL-HYB* encodes the chimeric CEL-CELP protein associated with chronic pancreatitis (63). Adapted from: *Fjeld et.al*. 2015. *Nat.Genet.*

CEL is the first lipase gene discovered to be associated with chronic pancreatitis (45). The chimeric CEL-HYB protein has a globular domain identical to the CEL-WT protein, while the C-terminal is made up by only 3 VNTR repeats, which originates from its pseudogene *CELP* (Figure 1.7). CEL-HYB showed reduced lipase activity, reduced secretion and intracellular retention when expressed in HEK293 cells (63). CEL-HYB has also shown to induce ER stress and autophagy (63, 65, 66). Taken together, these findings indicate that CEL-HYB is likely to

belong to the misfolding-dependent pathway of genetic risk in chronic pancreatitis (65, 66). Notably, most genetic risk variants of chronic pancreatitis have little effect by themselves. This is also the case for *CEL-HYB*, which means it works in combination with other risk factors to trigger disease, like tobacco smoking and pancreas divisum (65).

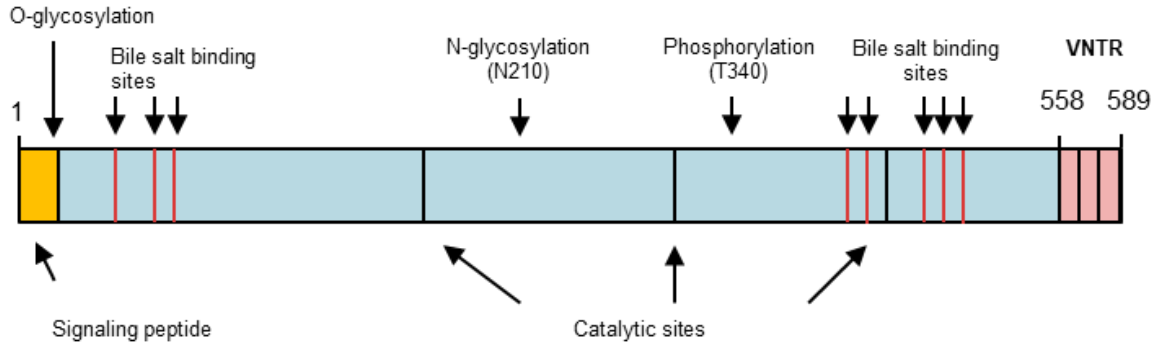

Figure 1.7 Structure of the CEL-HYB protein. The chimeric CEL-HYB protein has an identical globular domain to the CEL-WT protein, while the C-terminal is made up of only 3 VNTR repeats (pink), which originated from *CELP*. Adapted from *Fjeld.et.al.* 2015. *Nat.Genet.*

1.5.3 Other Pancreatic Diseases

Several genetic studies have investigated a possible link between *CEL* and pancreatic cancer. These studies included analysis of *CEL* single nucleotide polymorphisms (SNPs) (67), *CEL* VNTR insertion variants (68), *CEL*-VNTR length polymorphisms and *CEL* copy number variations (CNVs) (69), but no associations were found.

1.6 Protein degradation pathways

The degradation of proteins (proteolysis) is an important part of the cells' homeostasis and is a highly selective and regulated process (70). It is used as a quality-control system to ensure the quality of intracellular proteins by destructing misfolded or damaged polypeptides. There are two main pathways for proteolysis, namely the ubiquitin-proteasome system (UPS) and lysosomal degradation, also known as autophagy (70). The UPS is the main degradation pathway for small and short-lived proteins while larger proteins or aggregates are mainly degraded through autophagy (70). Recently, it has been shown to exist crosstalk between the two pathways. Both proteolytic pathways can be initiated by ubiquitylation, where ubiquitin gets covalently attached to the protein, and marks the protein for degradation (70).

1.6.1 Ubiquitin-proteasome system

Ubiquitylation starts with adenosine triphosphate (ATP)-dependent activation of ubiquitin by ubiquitin-activating enzyme (E1). The activated ubiquitin is then transferred to the cysteine residue of ubiquitin-conjugating Enzyme (E2) before the ubiquitin is transferred from E2 to the lysine-residue of the target protein by ubiquitin-ligase (E3). The target protein can be mono-ubiquitylated, multi-ubiquitylated or poly-ubiquitylated. The ubiquitylated protein is then recognized and degraded by proteasomes. The 26S proteasome is located in the cytoplasm and the nucleoplasm. It is a multi-catalytic protease complex which consists of several subunits controlled by different transcription factors. The ubiquitylated protein is captured by the subunit 19S regulatory particle. The subunit 20S core protease then cleaves the protein into short peptides (70, 71).

1.6.2 Autophagy

Autophagy can be divided into three major forms: macroautophagy, microautophagy and chaperone-mediated autophagy. Macroautophagy is the most common and will be further described here as autophagy (72). Autophagy can be selective or non-selective. Non-selective autophagy (bulk autophagy) is induced during starving conditions, while selective autophagy targets specific damaged organelles, invasive microbes, and misfolded proteins and aggregates (73). Autophagy starts by the formation of a double-membrane, called a phagophore, at ER-associated sites. The phagophore matures into an autophagosome which then fuses with the lysosome to become an autolysosome, where the degradation takes place (Figure 1.8). Regulation of the biogenesis and enclosure of autophagosomes are regulated by the ULK1 complex, and the BECLIN1 complex, which are under the regulation of mTOR complex 1 (mechanistic target of rapamycin complex 1), a well-known repressor of autophagy (70). Autophagy related proteins (ATGs) form a multimeric complex for the elongation of the autophagosomal membrane. One of the most important steps in autophagy induction is the attachment of phosphatidyl-ethanolamine to cytosolic LC3-I (microtubule-associated protein 1A/B-light chain 3-I). LC3-I is then transformed into LC3-II before it is recruited to the autophagosomal membrane. LC3-II binds to ubiquitin-binding autophagy receptors (e.g., p62), which are loaded with ubiquitylated cargo proteins. This ensures selective degradation (70). Autophagy is also regulated on a transcriptional level.

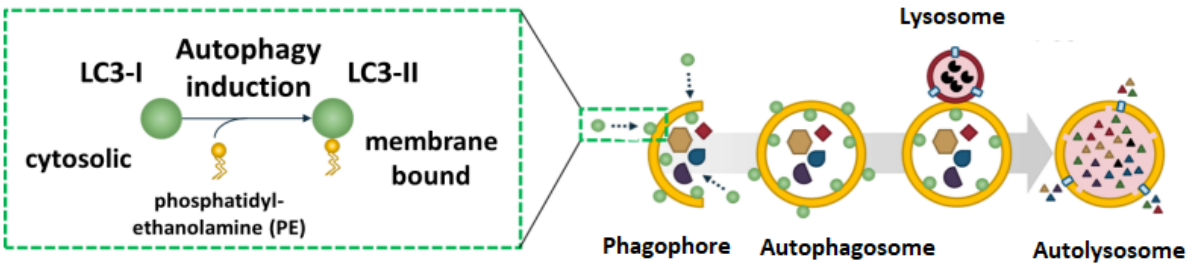

Figure 1.8. A schematic illustration of the mechanism of autophagy and the role of LC3. The double membrane, called a phagophore, matures into an autophagosome and then fuses with the lysosome to form an autolysosome. The degradation and recycling of macromolecules like long-lived proteins and protein aggregates takes place inside the autolysosome. *The figure is adapted from www.promega.com.*

2. Aims of the study

CEL is an extremely polymorphic gene for which several variants have been associated with pancreatic disease. The overall aim for this study was to understand the disease mechanism of one such pathogenic variant, namely the *CEL-HYB* allele.

The specific objectives of the project were:

1. To study the cellular fate of the CEL-HYB protein.
2. To identify CEL-HYB protein binding partners.

This project is part of a larger ongoing study in the Bergen CEL group.

3. Materials

Table 3.1 Plasmids

Plasmid*	Encoding	Description
pcDNA 3.1 CEL-WT/V5-His	CEL-WT	Plasmid expressing the CEL wild type (WT) protein containing a 16 VNTR region (Johansson et al., 2011)
pcDNA 3.1 CEL-HYB1/V5-His	CEL-HYB	Plasmid expressing the CEL-HYB protein (Fjeld et al., 2015)
pcDNA 3.1 CEL-TRUNC/V5-His	CEL-TRUNC	Plasmid expressing CEL-TRUNC, an artificial CEL protein lacking the VNTR domain (Johansson et al., 2011)
pcDNA 3.1/V5-His	EV	Empty vector

*All plasmids are based on the mammalian expression vector pcDNA3.1/V5-His B from Invitrogen

Table 3.2 Transformation, isolation, and purification of plasmid DNA

Product	Catalog number	Brand
Ampicillin sodium salt	A9518-5G	Sigma-Aldrich
One Shot TOP10 Chemically competent *E. coli*	C4040-03	Invitrogen
TE buffer, pH 8	A0386	Panreac Applichem
LB Broth (Lennox)	L3022	Sigma-Aldrich
ImMedia Amp Agar	45-0034	Invitrogen
SOC-medium	15544-034	Invitrogen
QIAGEN Plasmid Kit Midi (100)	12145	QIAGEN

Table 3.3 Sanger sequencing

Product	Catalog number	Brand
BigDye Terminator v1.1 Cycle Sequencing Kit	4337451	Applied Biosystems
Big Dye Terminator v1.1 & v3.1 5X Sequencing Buffer	4336701	Applied Biosystems
Betain	B0300	Sigma-Aldrich
Sephadex G-50 Superfine	G5050-50G	Sigma-Aldrich

*Primers are described in table 3.12

Table 3.4 Cell culturing

Product	Catalog number	Brand
HEK293 cells	632180	Clontech
Dulbecco's Phosphate Buffered Saline	D8537	Sigma-Aldrich
DMEM, high glucose w/pyruvate	41966029	Gibco
Trypsin-EDTA (0,05%), phenol red	25300-054	Gibco
Bambanker	302-14681	Lymphotec Inc.

Table 3.5 Cell transfection, cell lysis and protein concentration

Product	Catalog number	Brand
Opti-MEM®	37985-062	Gibco
Lipofectamine® 2000	11668-019	Invitrogen
10 X RIPA lysis buffer	20-188	Merck Millipore
Complete Protein Inhibitor Cocktail Tablet	11697498001	Roche
Pierce BCA protein assay kit	23225	Thermo Scientific
Microplate, 96 well, PS, F-bottom, clear	655101	Greiner Bio-One
Dulbecco's Phosphate Buffered Saline	D8537	Sigma-Aldrich

Table 3.6 SDS-PAGE, Coomassie staining and Western Blotting

Product	Catalog number	Brand
NuPAGE MOPS SDS Running Buffer (20X)	NP0001-02	Invitrogen
NuPAGE 4 to 12 %, Bis-Tris, 1.0 mm, Mini Protein Gel, 10-well	NP0321BOX	Invitrogen
NuPAGE 10 %, Bis-Tris, 1.5 mm, Mini Protein Gel, 10-well	NP0315BOX	Invitrogen
NuPAGE Transfer Buffer (20X)	NP0006-1	Invitrogen
Amersham Hybond P (PVDF membrane)	10600029	GE Healthcare
Blotto, non-fat dry milk	Sc-2324	Santa Cruz Biotechnology
NuPAGE LDS sample buffer (4X)	NP0007	Invitrogen
NuPAGE Sample Reducing Agent (10X)	NP0009	Invitrogen
Phosphate-Buffered Saline (PBS) tablets	18912-014	Gibco
Tween20	P1379	Sigma-Aldrich
Magic Mark XP Western Protein Standard	LC5603	Invitrogen
Precision Plus Protein Dual Color Standards	1610374	BioRad
Pierce ECL Western Blotting Substrate	32132	Thermo Scientific
XCell SureLock™ Mini-Cell	EI0001	Invitrogen
XCell II™ Blot Module	EI9051	Invitrogen
SimplyBlue SafeStain	LC6065	Invitrogen

Table 3.7 Antibodies

Product	Catalog number	Brand	Method
Anti-V5 antibody (mouse monoclonal)	R96025	Invitrogen	Western Blot and co-immunoprecipitation
Anti-GAPDH Antibody (0411) (mouse monoclonal)	sc-47724	Santa Cruz Biotechnology	Western Blot
Donkey anti-mouse IgG-HRP	sc-2318	Santa Cruz Biotechnology	Western Blot
Anti-CEL antibody (rabbit polyclonal)	HPA052701	Sigma-Aldrich	Immunohistochemistry

Anti-LC3B (D11) XP® (rabbit monoclonal)	3868	Cell Signaling	Immunohistochemistry and immunofluorescence
MACH3 Rabbit HRP-Polymer Detection	M3R531	BioCare Medical	Immunohistochemistry
As20.1, detecting CEL, (mouse monoclonal)		Generously provided by Prof. O. Hernell (Dept. of Clinical Sciences, Umeå University, Sweden	Immunofluorescence
Goat anti-Mouse IgG (H+L), Alexa Fluor™ 488	A11001	Invitrogen	Immunofluorescence
Goat anti-Rabbit IgG (H+L), Alexa Fluor™ 594	A11037	Invitrogen	Immunofluorescence

Table 3.8 Buffers and solutions

Buffer/Solution	Method	Composition
1X TBE buffer, pH 8.3	Gel electrophoresis	Tris-borate (89 mM) and EDTA (2mM)
Agarose gel, 1.5 %	Gel electrophoresis	100 ml TBE 1X buffer + 3 agarose tablets
1X RIPA Lysis buffer	Western Blot	1 ml 10X RIPA lysis buffer in 9 ml ddH_2O + 1 tablet Complete Mini EDTA-free protease inhibitors
1X SDS MOPS	Western Blot	For 1 L: 50 ml NuPage MOPS buffer (20X) in 950 ml ddH_2O
1X NuPage transfer buffer	Western Blot	For 1 L: 50 ml 20X NuPage transfer buffer and 100 ml methanol in 850 ml ddH_2O
PBS-Tween (0,05 %)	Western Blot	For 1 L: 2 tablets of PBS dissolved in 1 L ddH_2O + 0,5 ml PBS solution
5 % dry milk	Western Blot	5 g non-fat dry milk in 100 ml PBS-T (0,05 %)
IPH buffer, pH 8	Co-immunoprecipitation	50 mM Tris (pH 8,0), 150 mM NaCl, 5 mM EDTA, 1 % NP-40 in dH_2O, 1 tablet Complete Protein Inhibitor Cocktail Tablet pr 10 ml
Trypsin Buffer pH 7.8-8	Mass spectrometry	50 mM Tris, 1 mM $CaCl_2$ in ddH_2O
Dithiothreitol (DTT)	Mass spectrometry	100 mM in ddH_2O
Iodoacetamide (IA)	Mass spectrometry	200 mM in ddH_2O
Trypsin porcine, 0.1 µg/µl	Mass spectrometry	20 µg trypsin in 200 µl 2 mM tris pH 8.5
Acetonitrile/ Formic Acid (ACN/FA)	Mass spectrometry	70 % ACN containing 0.1 % FA in dH_2O
Trifluoroacetic acid (TFA)	Mass spectrometry	10%
Tris-EDTA, pH 9	Immunohistochemistry	10 mM EDTA, 10 mM Tris in dH_2O

Antibody diluent, pH 7.4	Immunohistochemistry	0.05M Tris, 0.15M NaCl, 1 % BSA, 0.02 % Na-azid, 0.05 % tween
2X HBS buffer, pH 7	Immunofluorescence	50 mM HEPES, 280 mM NaCl, 1.5 mM Na_2HPO_4 in dH_2O
0.2M Phosphate buffer, pH 7.2	Immunofluorescence	0.2 M Na_2HPO_4 + 0.2M NaH_2PO_4
Fixation solution	Immunofluorescence	0.1 M phosphate buffer pH 7.2, 4 % formaldehyde, in dH_2O
Wash buffer*	Immunofluorescence	1X PBS + 0.1 % Tween20
Permeabilization solution*	Immunofluorescence	Wash buffer + 0.1 % Triton X-100
Blocking solution*	Immunofluorescence	5 % goat serum in wash buffer
Glycine (1M) in PBS	Immunofluorescence	75.07 g glycine in 1 L PBS.
Hoechst in PBS?	Immunofluorescence	1 µl in 10 ml PBS

*Sterile filtered

Table 3.9 Co-immunoprecipitation

Product	Catalog number	Brand
Complete Protein Inhibitor Cocktail Tablet	11697498001	Roche
Dynabeads protein G Immunoprecipitation Kit	10007D	Invitrogen
DynaMag™ -2 Magnet	12321D	Invitrogen

Table 3.10 Animal models

Mouse model	Background	Generated by
Cel-HYB mouse strain	C57Bl/6N (Charles River Laboratories)	genOway

The transgenic Cel-HYB mouse strain has been developed by our research group. It is a humanized Cel-HYB *knock-in* strain, made on the C57BL/6J background, by genOway, Lyon, France. It was made by using the Cre/LoxP system.

Table 3.11 Genotyping of mice

Product	Catalog number	Brand
E.Z.N.A Tissue DNA Kit	D3396-02	Omega Bio-Tek
Multiplex PCR Kit	206143	QIAGEN
100 bp DNA ladder, 500µg/ml	N3231L	BioLabs
Gel loading buffer	G2526	Sigma-Aldrich
Elite 2 in 1 Agarose Tablets	PAL-E-2in1-100	Protein Ark

Table 3.12 Primers for genotyping of mice and Sanger sequencing of plasmids

Primers	Sequence (5'-3')
Genotyping	
196271cre-CHU2 (fwd)*	GCAAACTTCTTATTTATCCTCAAGCCTTGG
196272cre-CHU2 (rev)*	GTTATCGTCTTAGTGATGTCCAGGTAGTTGC
198353oth-CHU4 (WT allele)*	CGCAGAGCTGTCCAGGAGCACG
CELP VNTR-rev (CEL-HYB1 allele)*	CTGTGGAGGGCATGGAACT
Sanger sequencing	
DF (forward), exon 8	CCGCCGACATCGACTA
DR (reverse), exon 11	GCCGCTGTTTTCCGTA
T7 (forward), T7 promotor	ATTATGCTGAGTGATATCCC
BGH (reverse), BGH polyadenylated sequence	ATCTTCCGTGTCAGCTCC

*Sigma-Aldrich

Table 3.13 LC-ESI-MS

Product	Catalog number	Brand
Pierce BCA Protein Assay kit	23225	Thermo Scientific
Tris(hydroxymethyl)aminomethane	252859	Sigma-Aldrich
Calcium chloride x $2H_2O$	21097	Sigma-Aldrich
Dithiothreitol (DTT)	D-9163	Sigma-Aldrich
Iodoacetamide (IA)	I-6125	Sigma-Aldrich
Trifluoroacetic acid (TFA)	76-05-1	Sigma-Aldrich
NaCl	S7653	Merck
Trypsin porcine, 2 µg	V5111	Promega
96-well Waters Oasis HLB 96-well µElution Plate	186001828BA	Waters Corp

Table 3.14 Technical equipment and analytical software

Product	Brand	Method
NanoDrop™ One Microvolume UV-Vis Spectrophotometer	Thermo Scientific	Purification of plasmid DNA
GeneAmp® PCR System 2700	Applied Biosystems	Sanger sequencing
FinchTV chromatogram viewer	GeoSpiza, Inc	Sanger sequencing
3500xL Genetic Analyzer	Applied Biosystems	Sanger sequencing
Scepter™ 2.0 Handheld Automated Cell Counter	Millipore	Cell culturing
BioTek Gen5 2.06	Agilent	Protein concentration
Image Lab Software	Bio-Rad	Western Blot quantification
ChemiDoc™ MP Imaging System	Bio-Rad	Western Blot, Coomassie
Orbitrap Eclipse™ Tribrid MS	Thermo Scientific	Mass spectrometry
Ultimate 3000 RSLC system	Thermo Scientific	Mass spectrometry

Perseus 2.0.3.0 software	Max-Planck-Gesellschaft	Mass-spectrometry
CytoScape 3.9.1 software platform	CytoScape Consortium	Mass-spectrometry
FAIMS pro Interface	Thermo Scientific	Mass-spectrometry
Proteome Discoverer software	Thermo Scientific	Mass-spectrometry
Veriti™ 96 Well Thermal Cycler	Applied Biosystems	Genotyping
Fiji ImageJ	ImageJ Docs	Immunofluorescence
Leica TCS SP8 STED 3X	Leica microsystems	Immunofluorescence
Aperio ImageScope	Leica Biosystems	Immunohistochemistry
Nano Zoomer S60	Hamamatsu	Immunohistochemistry
Nano Zoomer XR	Hamamatsu	Immunohistochemistry
Tissue-Tek Prisma® Plus	Sakura	Immunohistochemistry

Table 3.15 Immunohistochemistry

Product	Catalog number	Brand
Phosphate-Buffered Saline (PBS) tablets	18912-014	Gibco
Tween20	P1379	Sigma-Aldrich
H2O2 30%	7722-84-1	Merck
DAB+ Chromogen, DAB+ substrate buffer	K3468	Dako
Hematoxylin	S3301	Dako
Protein Block Serum-Free Ready-To-Use	X0909	Dako
Pertex® Mounting Medium	00811-EX	HistoLab

Table 3.16 Immunofluorescence

Product	Catalog number	Brand
Calcium Chloride dihydrate	C7902	Sigma-Aldrich
Sodium pyruvate 100 mM (100X)	11360-039	Gibco
DMEM, no glucose	11966025	Gibco
Formaldehyde 16%	28908	Thermo Scientific
Phosphate-Buffered Saline (PBS) tablets	18912-014	Gibco
Tween™ 20 Surfact-Amps™ Detergent Solution	28320	Thermo Scientific
Goat serum	G9023	Sigma-Aldrich
Coverglasses, 18 mm Ø	WQ-0692	neoLabs
Prolong ™ Diamond Anti-Fade Mountant	P36961	Invitrogen

4. Methods

4.1 Preparation and sequencing of CEL-expressing plasmids

4.1.1 Bacterial cultures and plasmid purification

Transformed *E. coli* bacteria from glycerol stocks (provided by the group) was spread on LB agar plates with ampicillin and incubated overnight at 37 ºC. The following day, a single colony was picked for each variant, and added to 5 ml of LB medium and 5 µl of ampicillin (100 µg/ml). The preculture incubated at 37 ºC for 6-8 hours with rigorous shaking (250 rpm). Then the culture was diluted 1:1000 where 25 ml of LB medium was inoculated with 25 µl starter culture and 25 µl ampicillin (100 µg/ml). The culture incubated at 37 ºC for 14 - 16 hours with shaking (250 rpm). The next day, the cells were harvested by centrifugation at 21.300 x g for 40 minutes at 4 ºC. The supernatant was discarded, and bacterial pellet was used for plasmid purification.

Plasmid purification was performed according to the protocol of the QIAGEN Plasmid Kit midi (table 3.2). The bacteria pellet was resuspended in buffer P1 (resuspension buffer), then buffer P2 was added (lysis buffer). After incubating 5 minutes in room temperature (RT), buffer P3 (neutralization buffer) was added to the sample. The lysate was poured into the barrel of the QIAfilter Cartridge and incubated for 10 minutes at RT. QIAGEN-tip 100 was equilibrated by applying buffer QBT (equilibration buffer) and allowing the column to empty by gravity flow. Then the cap was removed from the cartridge and the plunger inserted. The lysate was filtered into the previously equilibrated QIAGEN-tip. The cleared lysate entered the resin by gravity flow. The QIAGEN-tip was washed twice with buffer QC (wash buffer). The DNA was eluted with buffer QF (elution buffer) into 50 ml Falcon tubes and precipitated by adding isopropanol. The sample was mixed and centrifuged at 21.300 x g for 45 minutes at 4 ºC. The supernatant was removed and discarded, and the pellet was washed with 70 % ethanol and centrifuged at 21.300 x g for 45 minutes at 4 ºC. The supernatant was discarded, and the pellet was left to dry for 5-10 minutes before it was redissolved in 200 µl 1X TE buffer and kept at RT to dissolve overnight.

4.1.2 Determination of plasmid concentration and quality

NanoDrop™ One Microvolume UV-Vis Spectrophotometer was used to determine the concentration of the purified plasmids. The absorbance of 1.3 µl eluate was measured at 260 nm. A 260/280 ratio of approximately 1.80 indicates a pure sample, while a lower ration would suggest protein or phenol contamination, and a higher ratio indicate RNA contamination. A

260/230 ratio between 2.0 and 2.2 also indicates a pure DNA sample. A lower ration would indicate phenol or guanidine residues. The DNA was stored at -20 ºC until further analysis.

4.1.3 Sanger sequencing

Sanger sequencing was performed to verify that the cDNA sequences of various CEL-expressing plasmids were correct. The PCR mastermix, primers and program are described in table 4.1, 3.12 and 4.2, respectively. The procedure was performed on Applied Biosystems 2720 Thermal Cycler. The PCR product was then cleaned using Sephadex G-50, to remove unincorporated primers and dNTPs. Sephadex was prepared one day before sequencing. First, Multiscreen 45 µl Column Loader was filled with Sephadex. Then, the Sephadex was transferred to an MS-HV plate. 300 µl dd H_2O was added to each well. The MS-HV plate was wrapped with plastic foil and stored at 4 ºC overnight. The next day the MS-HV plate was centrifuged at 910 x g for 5 minutes, and the PCR products (12 µl) and ddH_2O was added, followed by a subsequent centrifugation (910 x g for 5 minutes). The samples were collected in a 96-wells microtiter plate and sequenced on a 3500xL Genetic Analyzer.

Table 4.1 PCR Mastermix

Component	Volume (µl)
BigDye v.1.1	1
5X Big Dye Buffer	1
Betain	2
Primer 20 µM	0,25
PCR product	100 ng
ddH_2O	Fill up to 10 µl

Table 4.2 PCR thermal cycling process

	Temperature (ºC)	Time	Number of cycles
Pre-heat	96	1 min	
Denaturation Annealing Elongation	96 58 60	10 sec 5 sec 4 min	25
Hold	4	∞	

4.2 Cell culturing and transfection

4.2.1 Culturing of human embryonic kidney cells

Human embryonic kidney (HEK293) cells were cultured in Dulbecco's Modified Eagle's Medium (DMEM), supplemented with 10 % fetal bovine serum and 100 U/ml Antibiotic-

Antimycotic. If not stated otherwise, the cells were grown in T75 flasks in a humidified atmosphere at 37 ºC with 5 % CO_2.

4.2.2 Culturing of HeLa cells

HeLa cells were cultured in DMEM, supplemented with 10 % fetal bovine serum. If not stated otherwise, the cells were grown in T75 flasks in a humidified atmosphere at 37 ºC with 5 % CO_2.

4.2.3 Passaging and seeding of cells

The growth medium was removed, and the cells were carefully washed in 10 ml prewarmed PBS. Then 1 ml trypsin-EDTA was added for the cells to detach from the surface. The cells were resuspended in cell medium before a preferred amount was transferred to a new T75 flask, with pre-warmed cell medium, making a total of 12 ml. Scepter 2.0 Handheld Automated Cell Counter was used for counting cells.

4.2.4 Freezing and thawing protocol

For freezing, the cells were grown to 90 % confluency in a T75 flask, trypsinized and resuspended in 10 ml growth medium before centrifuged at 500 x g for 5 minutes at RT. The supernatant was discarded, and the cell pellet washed in 10 ml Dulbecco's Phosphate Buffered Saline (PBS) before centrifuged again at 500 x g for 5 minutes at RT. The supernatant was removed, and the pellet was resuspended in 10 ml Bambanker freezing media, aliquoted in cryotubes, á 1 ml, and frozen at -80 ºC short term, before moved to liquid nitrogen for long term storage. One vial of cells was thawed and transferred to a T25 flask containing 7 ml pre-warmed growth medium. The next day the medium was removed, and fresh growth medium added.

4.2.5 Transient transfection of HEK293 cells for western blotting (WB)

The day before transfection 4 x 10^5 cells were seeded in 6-well plates. After 24 hours the cells had grown to 60-70 % confluency. The cells were transfected with 10 µl Lipofectamine 2000 and 4 µg DNA. DNA and Lipofectamine 2000 were diluted in separate tubes with 250 µl OPTIMEM and incubated at RT for 5 minutes. The DNA solutions were then transferred to the tubes containing Lipofectamine 2000, and the mixture incubated at RT for 20 minutes. The samples were added to the cells and incubated for 4-6 hours before the transfection medium was removed and fresh growth medium added. The cells were subsequently grown for 24 hours.

4.2.6 Transient transfection of HeLa cells for immunofluorescence

HeLa cells (3 x 10^4 cells) were seeded on cover slips in 12 well plates. The cells incubated for 24 hours before they were transfected with plasmids containing EV, *CEL-WT*, *CEL-HYB* and

CEL-TRUNC. 60µl 2X HEPES (table 3.8) was added to a tube (solution A). 1 µg plasmid, 7.32 µl calcium chloride and ddH_2O up to 60 µl were added to another tube (solution B). Solution B was added slowly and dropwise to solution A while vortexing solution A. The mixed solution incubated at RT for 20 minutes before it was added directly to the cells by dripping it slowly and evenly into the medium. The cells incubated for 4-6 hours before the medium was removed and fresh growth medium added. The cells were subsequently grown for 48 hours before further analysis.

4.2.7 Transient transfection of HEK293 cells for co-immunoprecipitation

The day before transfection 5 x 10^6 cells were seeded in 10 cm petri dishes. After 24 hours the cells had grown to 60-70 % confluency. The cells were transfected with 15 µl Lipofectamine 2000 and 5 µg DNA. DNA and Lipofectamine 2000 was diluted in individual tubes containing 500 µl OPTIMEM and incubated at RT for 5 minutes. Subsequently, the DNA solutions were transferred to the tubes containing Lipofectamine 2000. The transfection solutions incubated at RT for 20 minutes. The transfection solutions were added to the cells and incubated for 4-6 hours before replacement with fresh growth medium. The cells were grown for 24 hours before further analysis.

4.3 Preparation of analytical fractions for western blotting

4.3.1 Preparation of cell lysate, pellet, and medium fractions

Twenty-four hours post transfection, 1 ml cell medium was collected on ice. The medium was centrifuged at 4 ˚C at 20.800 x g for 15 minutes. The supernatant was transferred to a new tube and analyzed as the medium fraction. The cells were washed in 1 ml ice-cold PBS before adding 150 µl ice-cold RIPA buffer. The cells were then collected on ice using a cell scraper. The samples incubated on ice for 30 minutes. They were then centrifuged at 20.800 x g for 15 minutes at 4 ˚C. The supernatant was transferred to a new tube and analyzed as the lysate fraction. The cell pellet was washed twice in 200 µl ice-cold PBS and centrifuged at 4 ˚C at 20.800 x g for 5 minutes, before 50 µl LDS 2X loading buffer was added to the pellet and the samples were denatured for 5 minutes at 95 ˚C. This was analyzed as the pellet fraction. The three fractions were stored at -20 ˚C for short-term storage, and -80 ˚C for long-term storage.

4.3.2 Determination of protein concentration

To determine total protein concentration of the lysate Pierce BCA Protein Assay kit was used and the manufacturer's protocol was followed. For detection BioTek Gen5 2.06 software was used.

4.4 Western blotting

4.4.1 SDS-PAGE

To prepare the medium and lysate fractions for SDS-PAGE 2 µl reducing agent, 5 µl LDS 4X and a total of 13 µl ddH_2O and sample were transferred to a tube. Sample size for all fractions corresponded to 5 µg total protein in the lysate fraction. The samples were denatured at 56 ºC for 15 minutes. The pellet fraction was prepared as described in section 4.3.1. For each fraction, 20 µl sample was loaded on Bis-Tris gels and separated by electrophoresis, using XCell SureLock Mini-Cell system. The gels ran in 1X MOPS buffer (table 3.8) at 90 V for 15 minutes, and then at 180 V until the dye front was at the bottom of the gel. 3 µl of Magic Mark XP and 5 µl of Precision Plus were used as protein size markers.

4.4.2 Western blotting

Following SDS-PAGE the proteins were transferred to a polyvinylidene fluoride (PVDF) membrane, using the XCell Blot Module system. The membrane was soaked in 100 % methanol 1 minute before use, for activation. Blotting was performed at 30 V for 60 minutes in NuPage transfer buffer with methanol (table 3.8). After blotting, the membrane was blocked in 5 % dry milk (table 3.8) at RT for 1 hour and then washed in PBS-T 0.05% for 3 x 5 minutes on a tilting laboratory shaker. All washes were performed this way, unless otherwise stated. Primary antibody, anti-V5 (1:20 000), recognizing the tagged CEL-protein, was added. As a loading control, anti-GAPDH (1:2000) was included. The antibodies were diluted in 1% dry milk (table 3.8). The membrane incubated with primary antibodies over night at 4 ºC on a tilting laboratory shaker. The following day, the membrane was washed, and the secondary antibody (1:5000) was added, and incubated for 1 hour at RT. Next, the membrane was washed before it was developed, using Pierce ECL Plus Western Blotting Substrate kit (table 3.6). For detection, ChemiDoc MP Imaging System was used.

4.4.3 Relative quantification of western blotting

To quantify the results, the western blot experiment was performed three times and the digital image data from the blots were analyzed by Image Lab Software (Table 3.14). First, the results

were normalized to GAPDH (total protein loading control). Second, the relative quantity was displayed as a ratio of the band volume (CEL-EV, CEL-HYB and CEL-TRUNC) divided by the reference band volume (CEL-WT). The significance of differences between the CEL variants in the different fractions were tested by unpaired t-test.

4.5 Immunofluorescence (IF)

4.5.1 Starvation of HeLa cells

48 hours post transfection, the cells were either normally fed by removing the growth medium and replaced with fresh medium, or starved for 2 hours, by removing the growth medium and replaced with growth medium without glucose, no bovine fetal serum, and added pyruvate (table 3.16).

4.5.2 Immunofluorescence of HeLa cells

The cells were washed in warm PBS. They were fixed in 1 ml 4 % formaldehyde diluted in 0.2M phosphate buffer, pH 7.2, (table 3.8) for 20 minutes. 1ml 1M glycine (table 3.8) was added to the well for 1 minute. The cells were rinsed twice in PBS, then permeabilized in permeabilization solution for 20 minutes at RT (table 3.8). The cells were washed in wash buffer (table 3.8), 3 x 5 minutes at RT on a rocking platform. All washes were performed in wash buffer at RT on a rocking platform unless stated otherwise. Then blocking solution was added (table 3.8) for 30 minutes at RT on a rocking platform. Primary antibody anti-As20.1 (1:200) or anti-LC3B (1:500) (table 3.7) was added. The antibodies incubated overnight at 4 degrees in a humidity chamber. The next day, the cells were washed 3 x 10 minutes before secondary antibody goat anti-mouse (1:200) or goat anti-rabbit (1:200) (table 3.7) was added. The cells incubated for 1 hour at RT. After incubation the cells were washed for 3 x 10 minutes. Then the cells were rinsed in PBS before adding Hoechst diluted in PBS (table 3.8) for 5 minutes in RT on a rocking platform. The cells were rinsed in PBS before mounting. The slides were left to set in RT for 24 hours in the dark, before stored at -18 ºC. Images were obtained on Leica TCS SP8 STED 3X.

4.6 Housing and genotyping of mice

4.6.1 Housing

The mice have been bred and housed at the Laboratory Animal Facility, Faculty of Medicine, University of Bergen. All mice work has been approved by the Norwegian Food Safety Authority (Mattilsynet), approval IDs FOTS 13902 (breeding) and FOTS 13510 (experiments). The experiments were conducted according to the European Convention for the Protection of Vertebrates Used for Scientific Purposes.

4.6.2 DNA extraction

A mouse ear sample was taken by the Laboratory Animal Facility at the University of Bergen. The tissue was stored at -20 ºC until genotyping was performed. The DNA extraction procedure follows the protocol of E.Z.N.A Tissue DNA Kit. To make sure DNA was extracted from the samples, the concentration was determined using Nanodrop spectrophotometer (section 4.1.2).

4.6.3 Polymerase Chain Reaction (PCR)

Extracted DNA was amplified using PCR. A general PCR was used to differentiate between wild type ($Cel^{+/+}$), heterozygous knock-in ($Cel^{HYB/+}$), and homozygous knock-in ($Cel^{HYB/HYB}$) of the mouse *Cel*-locus. I addition, an allele specific PCR reaction was performed to amplify and confirm the presence of the VNTR region of Cel-HYB. The reaction mix consisted of 12.5 µl mastermix (table 3.11), 1.5 µl forward primer, 1.5 µl reverse primer, 7.5 µl ddH_2O and 2 µl DNA template. Primers are listed in table 3.12. The PCR thermal cycling conditions are listed in tables 4.3 and 4.4.

Table 4.3 General PCR thermal cycling process

	Temperature (ºC)	**Time**	**Number of cycles**
Pre-heat	95	15 min	
Denaturation Annealing Elongation	94 65 72	60 sec 90 sec 90 sec	35
Final extension Hold	72 4	10 ∞	

Table 4.4 Specific PCR thermal cycling process

	Temperature (ºC)	Time	Number of cycles
Pre-heat	95	15 min	
Denaturation Annealing Elongation	94 65 72	30 sec 30 sec 5 min	30
Final extension Hold	72 4	8 ∞	

4.6.4 Agarose gel electrophoresis

The PCR products were run on a 1.5 % agarose gel. 7 µl PCR product and 3.5 µl gel loading buffer was mixed and loaded onto the gel. The gel ran in Tris/Borate/EDTA (TBE) buffer, at 125 V for 30 minutes. The gel bands were visualized using ChemiDoc MP Imaging System.

4.7 Isolation of the mouse pancreas

4.7.1 Starvation of mice

The mice were starved for 24 hours, fed for two hours, then starved again for 24 hours immediately before being euthanized.

4.7.2 Isolation of the mouse pancreas

Mice were sacrificed by carbon dioxide (CO_2) overdose, with a flow rate of 30-70 % of cage volume per minute. The mouse was placed in dorsal recumbency. To isolate the pancreas, the skin was wet with 70 % alcohol, and a cut was made through the skin and abdominal wall, from the sternum to the caudal abdomen, following the midline. The cut was extended laterally from the caudal abdomen to each side, and the abdominal muscles and skin were peeled back for better vision and access to the pancreas. The colon was moved aside to visualize the pancreas. Pancreas was then dissected out, including the spleen on its left side and the major duodenal papilla on its right side. The pancreas was fixed in 4 % formaldehyde overnight at RT. It was then embedded in paraffin and sectioned (3-5 µm) onto Superfrost microscope slides and dried overnight at 56 ºC.

4.8 Hematoxylin and eosin (HE) staining and immunohistochemistry (IHC)

One slide from each paraffin embedded mouse pancreas was H&E stained by Sakura Prisma Plus (table 3.14) for histology. The rest of the slides were stored at 4 ºC until used for immunohistochemistry.

4.8.1 Immunohistochemistry

The slides incubated at 56 ºC for 15 minutes. Then the slides were deparaffinated in xylene for 2 x 5 minutes, 100% ethanol 2 x 2 minutes, 96% ethanol 2 x 2 minutes, 80% ethanol 2 x 2 minutes and dH_2O for 1 minute. The slides were then placed in PBS-T (0.05%) before they incubated in a pressure chamber in Tris-EDTA pH 9 (table 3.8), at 120 ºC for 1 minute. After incubation the slides cooled down in room temperature before rinsed with dH_2O. The slides were washed in PBS-T (0.05%) (table 3.8) for 3 x 5 minutes. All washes were performed in PBS-T (0.05 %) and on a rocking platform unless stated otherwise. The tissues were delineated with ImmEdge Hydrophobic Barrier Pen, before blocked with protein block for 8 minutes at RT. The protein block was removed and the primary antibody anti-CEL (1:200) or anti-LC3B (1:200) was added. The slides incubated in humidity chamber at 4 ºC overnight. The next day the primary antibody was removed, and the slides washed for 4 x 15 minutes. The slides then incubated with 3 % H_2O_2 for 5 minutes at RT. The slides were rinsed in dH_2O and washed for 3 x 5 minutes. Probe MACH3 was added and incubated for 20 minutes. The slides were then rinsed in dH_2O and washed for 3 x 5 minutes. HRP polymer MACH3 was added and incubated for 20 minutes. Then the slides were rinsed in dH_2O and washed for 15 + 30 + 15 minutes. For visualization, 3,3'-diaminobenzidine (DAB) was used, 1 minute for anti-CEL and 3 minutes for anti-LC3B. The sections were stained with hematoxylin for 10 minutes in RT. The slides were dehydrated in 80%, 96% and 100% ethanol for 1 minute each, and then in xylene for 2 minutes. The tissues were then mounted. Images were obtained by either Nano Zoomer S60 or Nano Zoomer XR and Aperio ImageScope software (table 3.14).

4.9 Co-Immunoprecipitation

4.9.1 Lysis of transfected cells

The day after the cells had been transiently transfected (section 4.2.7), the medium was discarded, and the cells washed in 5 ml ice-cold PBS. 500 µl of IPH lysis buffer (table 3.8) with protein inhibitor was added to the cells. The cells were collected on ice using a cell scraper and

transferred to a tube, which was placed on a rotating wheel at 4 ºC for 20 minutes, followed by centrifugation at 17.900 x g for 10 minutes at 4 ºC.

4.9.2 Pre-clearing of the lysate

Dynabeads were vortexed for 30 seconds to make a homogenous suspension. 50 µl were transferred to a tube, which then was placed on the magnetic rack. The supernatant was discarded. The beads were washed in 200 µl Washing Buffer (table 3.9), by rotation for 1 minute at RT. 650 µl cell lysate was added to the washed beads and incubated on a rotating wheel for 1 hour at 4 ºC.

4.9.3 Co-Immunoprecipitation (Co-IP)

The co-immunoprecipitation procedure was performed according to the protocol in the Dynabeads Protein G Immunoprecipitation Kit. The Dynabeads were vortexed for 30 seconds to make a homogenous suspension. 50 µl were transferred to an Eppendorf tube, which then was placed on a magnetic rack. The supernatant was removed. 6 µg anti-V5 antibody, was added to 200 µl Antibody Binding and Washing Buffer. This was then added to the tube containing the beads, while off the rack. The sample incubated on a rotator at RT for 10 minutes. The supernatant was discarded while on the magnetic rack. 200 µl Ab Binding and Washing Buffer was added and beads were washed by carefully pipetting up and down, using pipettes with clipped off ends. All washes were performed like this, unless stated otherwise. The tube was placed in the rack and the supernatant was discarded. 650 µl of pre-cleared lysate was added to the Dynabeads-antibody complex. The sample incubated on rotator at RT for 10 minutes. The tube was placed on the rack and the supernatant was transferred to new Eppendorf tubes, for further analysis of the unbound sample. The Dynabeads-antigen-antibody complex was washed three times. The beads were resuspended in 100 µl Washing Buffer and transferred to a clean Eppendorf tube. The buffer was discarded, and the beads resuspended in 50 µl ddH_2O, and stored at – 20 ºC until mass spectrometry was performed. When doing co-IP for Coomassie staining and WB the washing buffer was removed while on rack, and 20 µl elution buffer and 10 µl 4X LDS was added. The samples were denatured at 70 ºC for 10 minutes. Then stored at - 20 ºC until further analysis.

4.9.4 Coomassie G-250 stain of immunoprecipitated proteins

10 µl of the sample was separated by SDS-PAGE (section 4.4.1), and the gel washed in ddH_2O for 3 x 5 minutes. Then the gel incubated in SimplyBlue SafeStain at RT for 1 hour on a tilting laboratory shaker. The stain was discarded, and the gel washed in ddH_2O for 1 hour, then ddH_2O

was changed and the gel washed for one more hour. For detection of the protein bands, ChemiDoc MP Imaging System was used.

4.9.5 Western Blot of immunoprecipitated proteins

After thawing the samples, they were heated to 70 ºC for 10 minutes. The tube was placed on the magnetic rack and 10 µl of the supernatant was loaded on to the gel. The gel ran in 1X MOPS buffer (table 3.8) at 90 V for 15 minutes, and then at 180 V until the dye front was at the bottom of the gel. The WB procedure is described in detail in section 4.4.2. The primary antibody used was anti-V5 (1:20 000).

4.10 Liquid Chromatography-Electrospray Ionization-Mass Spectrometry (LC-ESI-MS).

The LC-ESI-MS was performed in collaboration with the Proteomics Unit at the University of Bergen (PROBE), which is a national core facility for large scale protein analysis using mass spectrometry. Thus, I prepared the samples while the facility performed the mass spectrometry. PROBE was also involved in the data analysis.

4.10.1 Sample preparation

Digestion. To digest the immunoprecipitated proteins attached to the magnetic beads, the samples were placed on a magnetic rack for 1 minute and the supernatant discarded. 40 µl trypsin buffer and 4 µl 0.1M DTT was added, and the samples denatured at 95ºC for 5 minutes with rigorous shaking (1200 rpm). The samples were room tempered and added 5 µl 0.2M IAA before incubated at 22 ºC for 1 hour (1200 rpm). Then, 0.8 µl 0.1M DTT was added followed by incubation at 22 ºC for 10 minutes (1200 rpm). Finally, 10 µl trypsin porcine (0.1 µg/µl) (table 3.8) was added to the samples, and the samples incubated at 37 ºC over night (1200 rpm).

Peptide extraction. The following day, the samples were centrifuged at 13.000 rpm at 24 ºC for 3 minutes and placed on a magnetic rack. After one minute the supernatant was transferred to a low protein binding collection tube. To the beads, 50 µl 0.5M NaCl was added and mixed, until all beads were in suspension. The samples were then sonicated in a water bath for 30 seconds, before centrifuged at 13.000 rpm at 24 ºC for 3 minutes. Next, the samples were placed on a magnetic rack, and after 1 minute the supernatant was transferred to the same low protein binding collection tube as above. Finally, 6 µl TFA (10 %) was added to the samples

to acidify them, acidic pH was confirmed using pH indicator paper. Each sample made up a total volume of 120 µl.

Desalting. Peptides were desalted in the OASIS® HLB µElution Plate. The columns were first wetted and centrifuged, before conditioned and centrifuged (Table 4.5). Each sample (120 µl) was diluted in 380 µl TFA 0.1 % (total 500 µl), before added to the conditioned columns for sample binding, following centrifugation of the plate (Table 4.5). The collected samples were then cleaned and centrifuged before they were eluted from the columns (Table 4.5). The collected samples of 200 µl were transferred to clean low protein binding collection tubes. Then the samples were dried on a freezeVac before subjected to mass spectrometry.

Table 4.5 Desalting of peptides using the OASIS® HLB µElution Plate.

Procedure	Added to columns	Centrifugation
Column wetting	500 µl ACN/FA (table 3.8)	200 x g - 1 minute
Column conditioning*	500 µl TFA 0.1% (table 3.8)	200 x g - 1 minute
Sample binding	500 µl prepared sample	100 x g - 4 minutes
Sample cleaning**	500 µl TFA 0.1% (table 3.8)	200 x g - 1 minute
Sample elution*	100 µl ACN/FA (table 3.8)	200 x g - 1 minute

*repeated once
**repeated twice

4.10.2 LC-ESI-MS and raw data processing by PROBE

LC-ESI-MS and raw data processing was performed by PROBE as described elsewhere (74). Samples containing tryptic peptides were injected into an Ultimate 3000 RSLC system, coupled to the Orbitrap Eclipse™ Tribrid mass spectrometer, consisting of an EASY-IC/ETD/PTCR ion source, and a FAIMS Pro Interface. To search the raw LC-MS/MS files in Proteome Discoverer software v2.5, SEQUEST HT database search engine was used, with Percolator validation (FDR < 0.1). The search was conducted against the downloaded reviewed Swiss-Prot human database, using default settings. The data was normalized by using the sum of all peptide amounts. To calculate the protein abundance, sample abundances of the connected peptide groups were summed up.

4.10.3 Data and bioinformatics analyses

Qualitative comparison of the replicates was performed by Venny 2.1 Venn Diagram. Further data analysis and visualization were performed in Perseus version 2.0.3.0. Normalized values were filtered by protein false discovery rates (FDR) confidence of 1% or less, and by excluding

true contaminants. The values were log_2 transformed. Samples with 2 or fewer replicates with valid numbers were removed. Hierarchical clustering and heat mapping of significantly differential proteins was performed using Pearson Correlation and average linkage. Protein-protein interaction networks (PPIs) were obtained by using the STRING database version 11.5, with interactions derived from experiments and databases at a high confidence score of 0.7. Networks were visualized using the Cytoscape platform version 3.9.1. The ClusterONE plugin was used to identify protein clusters of high cohesiveness.

5. Results

5.1 The cellular fate of the CEL-HYB protein – at the cellular level

Based on current knowledge, CEL-HYB is less secreted than the normal CEL protein and tend to accumulate inside the cells (63). Expression of CEL-HYB has also shown to increase autophagy, suggesting that autophagy may serve as the degenerative pathway of the protein and autophagic dysfunction may be the key initiating event in pancreatitis.

Here we wanted to investigate these findings in more detail by using both cellular and mouse model systems.

5.1.1 Protein structure of CEL variants analyzed in this study

A schematic overview of the different CEL protein variants studied is presented in Figure 5.1. For the normal CEL protein (CEL-WT) a variant with 16 VNTR repeats was used. Then, in addition to CEL-HYB, an artificial variant (CEL-TRUNC), was included as a control to study the biological effects of an absent VNTR region. All three variants were V5-tagged.

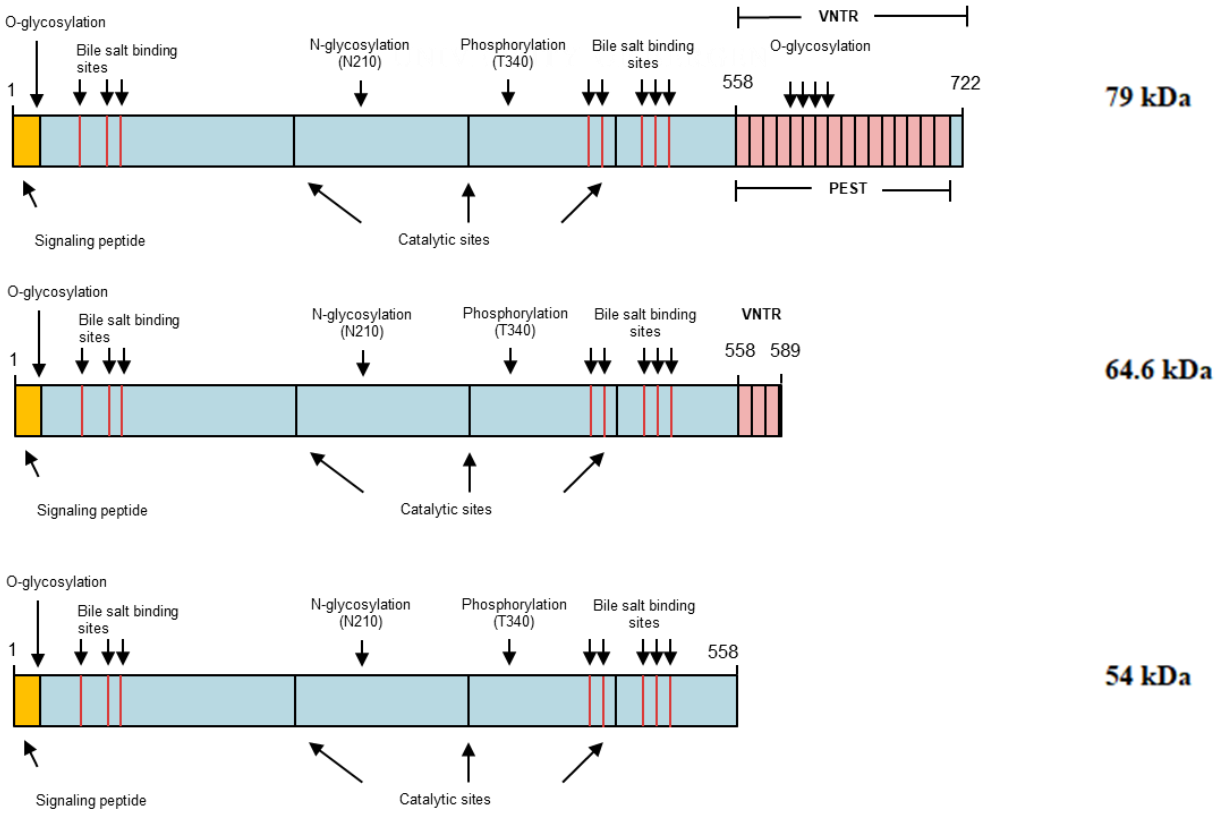

Figure 5.1. Schematic overview of CEL protein variants. The three variants CEL-WT (upper), CEL-HYB (middle) and CEL-TRUNC (lower) have identical globular domain (light blue) and signaling peptide (yellow). The VNTR region (pink) has 16 repeats in CEL-WT, 3 repeats in CEL-HYB, whereas CEL-TRUNC lacks a VNTR region. Their theoretical molecular weights are listed to the right. Adapted from *Fjeld.et.al.* 2015. *Nat.Genet.*

5.1.2 Isolation and sequencing of CEL-expressing plasmids

Before analysis of CEL in cellular systems, plasmids expressing CEL-WT, CEL-HYB or CEL-TRUNC were prepared using the QIAGEN plasmid kit (section 4.1.1). In addition, an empty vector (EV) was included as a negative control. The plasmid concentration and quality were estimated and confirmed by OD measurements (section 4.1.2). For verification of the CEL cDNA sequence, Sanger sequencing was performed (Section 4.1.3) (data not shown).

5.1.3 Cellular fractionation of CEL variants in HEK293 cells

HEK293 cells were transiently transfected with *CEL-WT*, *CEL-HYB* or *CEL-TRUNC* constructs as well as EV (section 4.2.5). After 24 hours, the medium, cell lysate and insoluble pellet fractions were isolated and analyzed by western blotting (section 4.4.2). The CEL proteins were detected by using an anti-V5 antibody and anti-GAPDH was included for monitoring protein loading. The experiment was performed three times and a representative blot is shown in Figure 5.2.A.

In the lysate fraction, CEL-WT was detected as a strong band between 100 kDa and 120 kDa. In addition, two weaker bands were observed at about 80 kDa and 90 kDa (Figure 5.2.A). CEL-HYB was seen as one diffuse band at just above 60 kDa, whereas CEL-TRUNC was observed as two bands just below 60 kDa. Compared to CEL-WT, the bands of CEL-HYB and CEL-TRUNC were less intense, suggesting lower amount of proteins. The different band sizes observed for all three variants most likely represent different glycosylated forms of the CEL proteins (75, 76). In the insoluble pellet fraction, more intense bands were detected for both CEL-HYB (at about 65 kDa) and CEL-TRUNC (at about 60 kDa), compared to CEL-WT (at about 110 kDa). For CEL-HYB and CEL-TRUNC we also found high molecular weight bands at about 130-140 kDa, that may represent aggregated forms of the proteins. As for the medium fraction, there was a strong band for CEL-WT and only weaker bands for CEL-HYB and CEL-TRUNC, indicating retention of the two latter variants.

Quantification of the expression of CEL variants in different analytical fractions confirmed that CEL-HYB and CEL-TRUNC were found in very low amounts in both the lysate and medium fractions, compared to the wildtype protein (Figure 5.2.B). There is a statistical significance between CEL-HYB and CEL-TRUNC, compared to CEL-WT in the lysate and medium fractions ($p < 0.0001$). For the insoluble pellet fraction, there was about 3-fold increase in CEL-HYB and about 1.5-fold increase in CEL-TRUNC, compared to CEL-WT. Taken together, these findings correspond well with previous studies on CEL-HYB (63, 77).

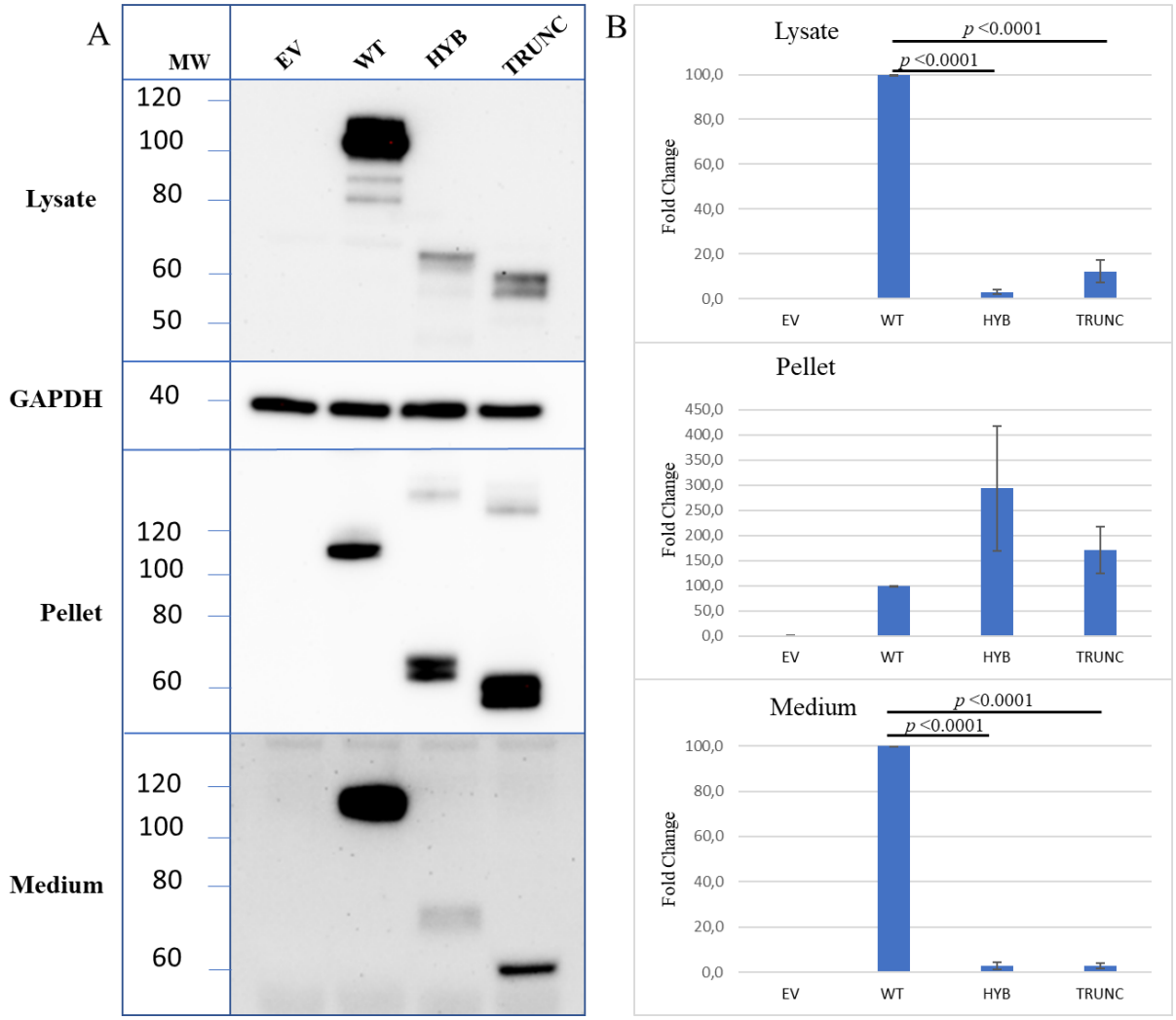

Figure 5.2 A) Expression and secretion of CEL variants in transfected HEK293 cells. Cells were transiently transfected with empty vector (EV) and V5-tagged *CEL-WT*, *CEL-HYB* and *CEL-TRUNC*. Medium, lysate and pellet fractions were analyzed by SDS-PAGE and western blotting using an anti-V5 antibody. GAPDH was used as loading control. The blots shown are representative of three independent experiments**. B)** Quantification of the band intensities in the western blots. The intensity of the CEL bands were adjusted to GAPDH and normalized to CEL-WT. Error bars are standard error of the mean (SEM) of three independent experiments.

5.1.4. Immunostaining of CEL and the autophagy marker LC3B in HeLa cells

To investigate the link between CEL and autophagy in more detail, the cellular distribution of CEL and the autophagy marker LC3B were analyzed by immunostaining followed by confocal imaging. We also wanted to see if CEL colocalized with LC3B. For this experiment we used HeLa cells that were transiently transfected, to examine if CEL and LC3B co-localized in the cells. HeLa cells were transiently transfected with EV, *CEL-WT, CEL-HYB* or *CEL-TRUNC* before either starved (24 hours) or continued fed, followed by fixation, immunostaining, and analysis by confocal microscopy (section 4.5). Starvation of the cells was used to enhance the autophagy process (72).

For detection of CEL, the anti-As20.1 antibody was used, detecting the globular domain of the protein. Alexa-fluor 488 was used as secondary antibody. As shown in Figure 5.3.A, the CEL protein was detected (in green) in transfected cells. Overall, the CEL signal was strongest in the Golgi apparatus and weaker in the endoplasmic reticulum. In Figure 5.3.B, the images have been overexposed to study more details of the CEL distribution. In fed cells expressing CEL-WT, there was punctuate-like staining of CEL proteins towards the cell membrane. For cells expressing CEL-HYB and CEL-TRUNC, the puncta became larger, and they increased in number. A similar pattern was observed in the starved cells for all three CEL variants, displaying punctuate-like structures of the CEL proteins. In addition, we observed an increased cell-death in cells expressing CEL-HYB, compared to the other CEL variants or EV.

For detection of LC3B, a primary anti-LC3B antibody and a secondary anti-Alexa-fluor 594 antibody were used. Positive staining for LC3B was observed (in red) as perinuclear punctuate-like structures, with less signal in cells transfected with EV compared to CEL-expressing constructs (Figure 5.4). There were no obvious differences in expression pattern between CEL-variants or between fed and starved cells. We also performed double-staining for CEL and LC3B, but unfortunately the experiment failed due to technical problems.

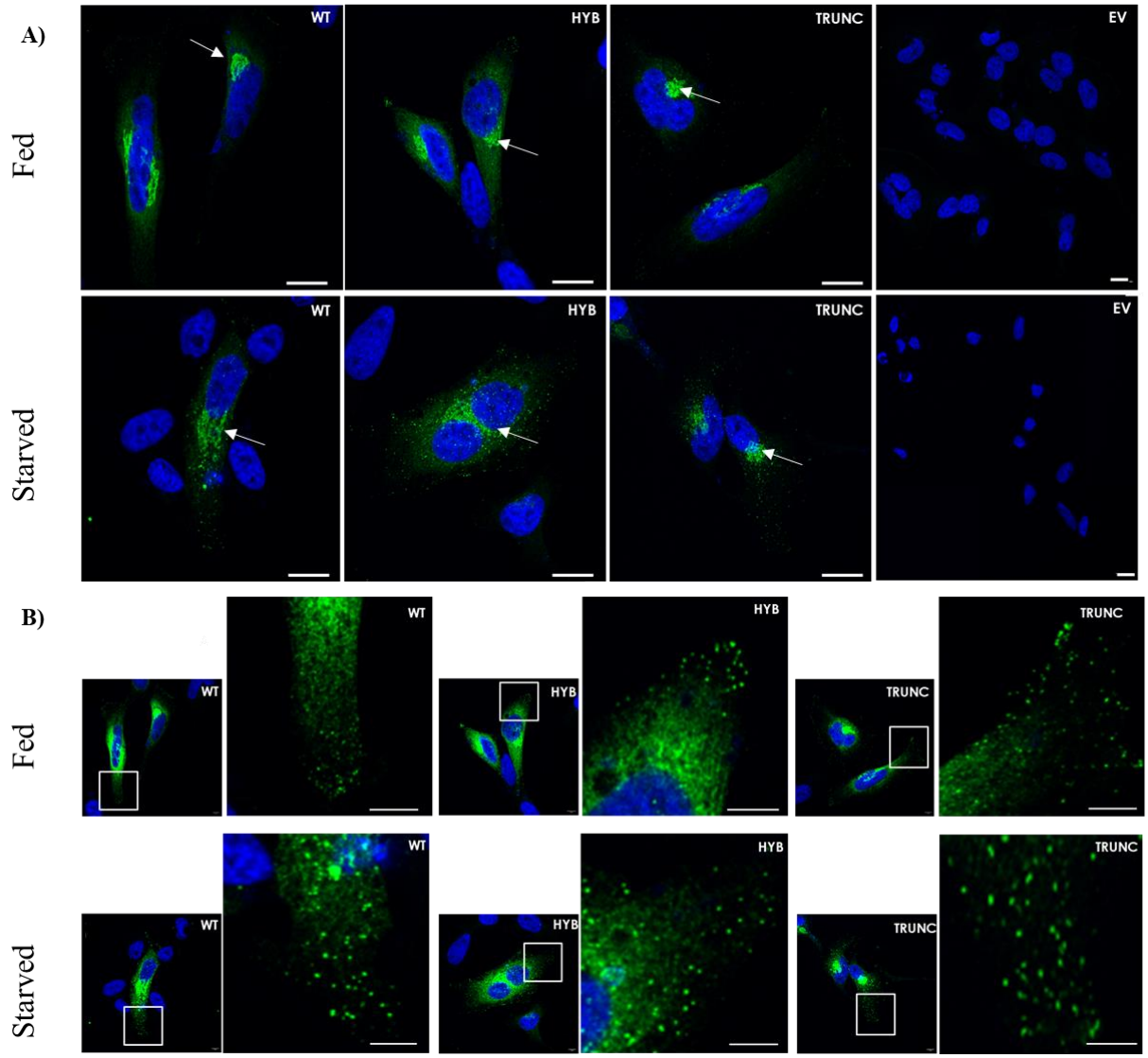

Figure 5.3. Intracellular distribution of CEL protein variants in fed and starved HeLa cells. A) HeLa cells transiently transfected with EV, *CEL-WT*, *CEL-HYB* or *CEL-TRUNC* were stained using anti-As20.1 antibody (detecting CEL), and Alexa-Fluor-488 (green) as secondary antibody. EV was included as negative control. The chromosome counterstain (Hoechst) is shown in blue. Each image represents a maximum intensity projection of a z-stack taken through the entire depth of the cell. CEL is dispersed in the reticular ER and accumulated in the Golgi apparatus (white arrows). *Scale bar: 15 µm*. **B)** Magnification and over exposure of the images in Figure 5.A. *Scale bar: 6 µm.*

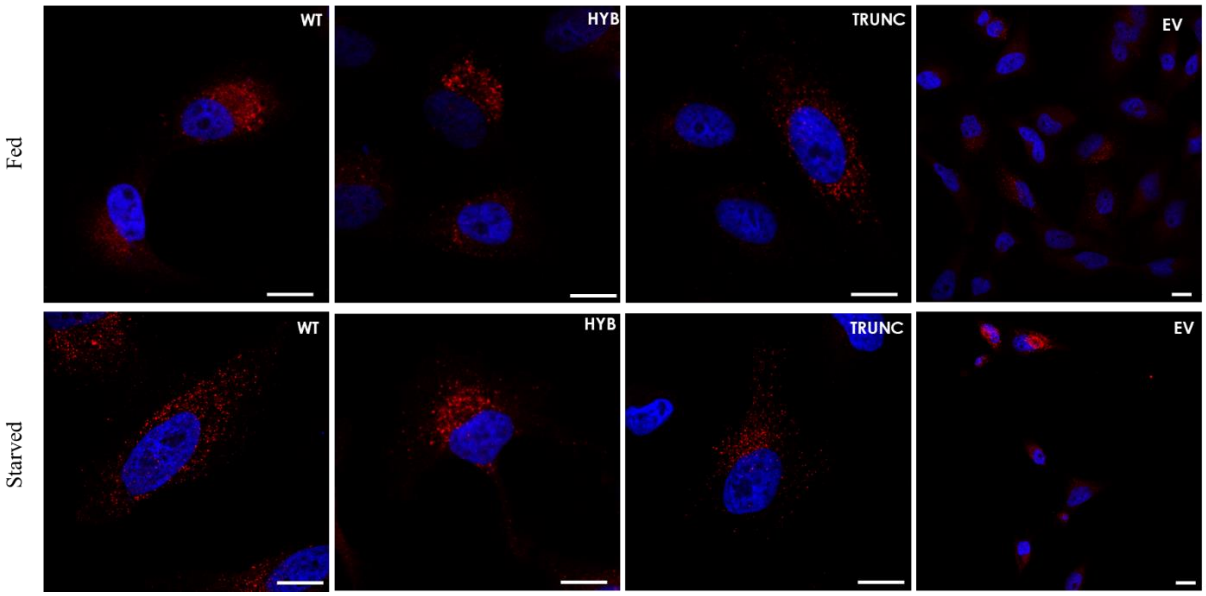

Figure 5.4. Intracellular distribution of LC3B-II in fed and starved HeLa cells. HeLa cells transiently transfected with EV, *CEL-WT*, *CEL-HYB* or *CEL-TRUNC* were immunostained using the anti- LC3B antibody (1:500). Alexa-Fluor-594 (red) was used as secondary antibody. EV was included as negative control. The chromosome counterstain (Hoechst) is shown in blue. Each image represents a maximum intensity projection of a z-stack taken through the entire depth of the cell. *Scale bar: 15 µm.*

5.2 The cellular fate of the CEL-HYB protein – at the organ level

5.2.1 Genotyping of the Cel-HYB mouse model

Before analyzing the mice, all animals were genotyped by PCR followed by agarose gel electrophoresis (section 4.6). Two PCR reactions were performed: one general to distinguish between control ($Cel^{+/+}$), heterozygous ($Cel^{+/HYB}$) and homozygous ($Cel^{HYB/HYB}$) Cel-HYB mice, and one allele-specific PCR to amplify and confirm the presence of the *Cel-HYB* allele. For the general PCR, the expected band sizes for the *Cel* wild-type and *Cel-HYB* allele were 303 bp, and 394 bp, respectively. As for the specific PCR, the predicted band size was 300 bp. In Figure 5.5, genotyping results of five mice are represented: three heterozygous animals, one homozygous for the *Cel-HYB* allele, and one with only the normal mouse *Cel* alleles (control).

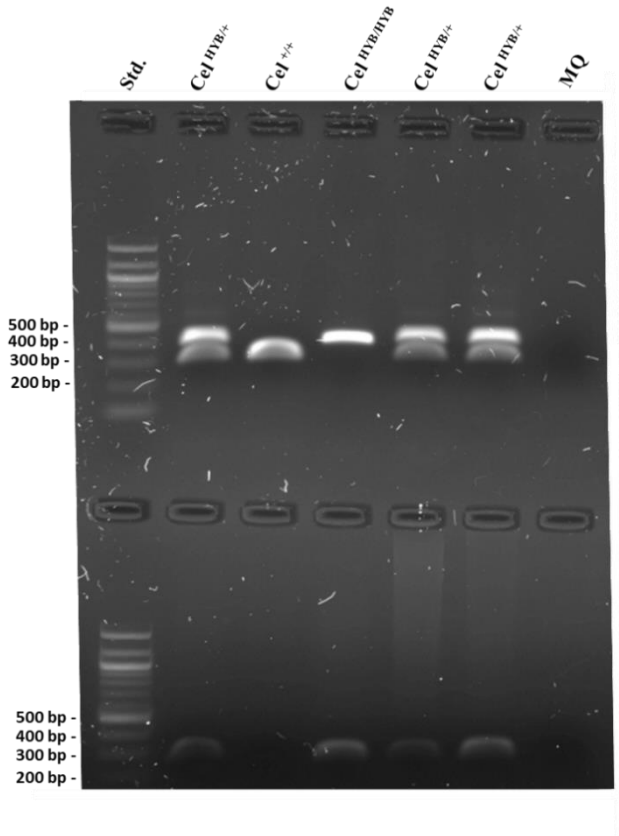

Figure 5.5: Genotyping of Cel-HYB mice. Agarose gel (1.5 %) electrophoresis of PCR products from five Cel-HYB mice, three of which were heterozygous ($Cel^{HYB/+}$) , one homozygous ($Cel^{HYB/HYB}$) , and one control mouse ($Cel^{+/+}$) . Std: 100 bp DNA ladder, MQ: ultrapure water (negative control).

5.2.2 Histology of the Cel-HYB mouse pancreas

The cellular distribution of CEL-HYB has so far only been investigated in cell lines. To take our research to a new level, we wanted to study CEL-HYB in pancreatic tissue. To do so, we took advantage of a humanized Cel-HYB mouse model that develop CP spontaneously (Fjeld et al, unpublished). Compared to control mice, the pancreas in heterozygous Cel-HYB mice showed infiltration of fat and mononuclear inflammatory cells (Figure 5.6). In homozygous Cel-HYB mice, in addition to fatty infiltration and inflammatory cells, there was also loss of acinar cells, and likely interlobular fibrosis (Figure 5.6), all of which are histological features of chronic pancreatitis.

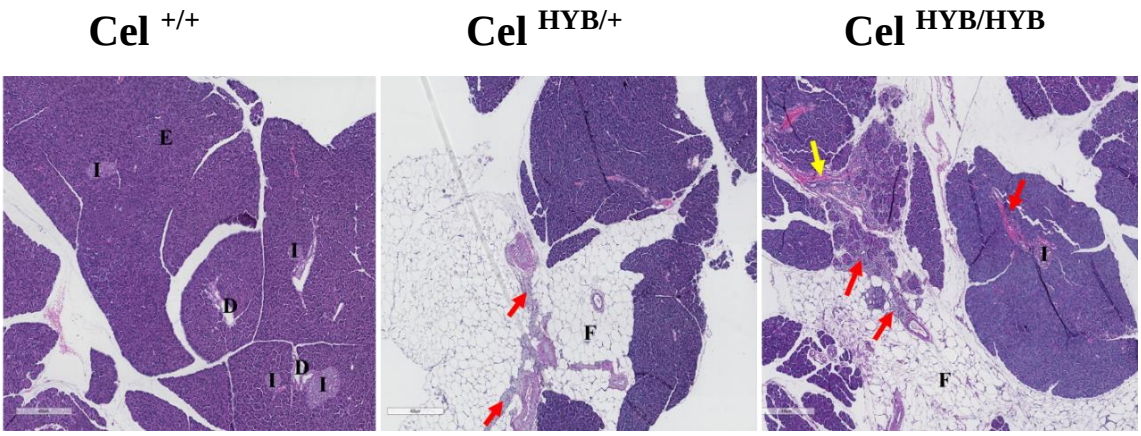

Figure 5.6 Pancreas histology of 6-month-old heterozygous and homozygous Cel-HYB mice, and a control mouse. HE-stained pancreatic tissue of male mice. Heterozygous and homozygous Cel-HYB mice show features of chronic pancreatitis, like infiltration of fat and inflammatory cells. I: islets of Langerhans. D: pancreatic ducts. F: fat infiltration. Red arrows: inflammatory cells. Yellow arrow: fibrosis. *Scale bar 400 µm.*

5.2.3 Immunohistochemistry for detecting Cel and LC3B in Cel-HYB mice.

To analyze expression of Cel and LC3B in mouse, pancreatic tissue sections from starved and fed Cel-HYB and control mice (6 months of age) were analyzed by IHC (section 4.8.1). Notably, the mice were starved for studying LC3B (autophagy), but the same mice were also analyzed for Cel-expression as described below.

Cel staining was mainly observed in the pancreatic acinar cells of all mice (Figure 5.7). Moreover, positive staining was seen as small dot-like structures, suggesting storage of Cel proteins in zymogen granules. For the fed mice, Cel was expressed evenly throughout the apical part of the acinar cells in the control. In contrast, in the heterozygous Cel-HYB mouse, the proteins were aligned in a row along the cell membrane, forming a tubular pattern (Figure 5.7). In addition, the staining was more intense and the dot-like structures larger, which may suggest accumulation and aggregation of the Cel protein. The same pattern was seen for the homozygous Cel-HYB mouse. Interestingly, when starving the mice, the controls showed a tubular expression pattern similar to the fed Cel-HYB mice (Figure 5.7). For the starved heterozygous and homozygous Cel-HYB mice, the same tubular Cel expression pattern was continued for. Thus, starving the mice influences the distribution of zymogen granules in the acinar cells. The pattern was found in the majority of the pancreas sections for the starved homozygous and heterozygous mice.

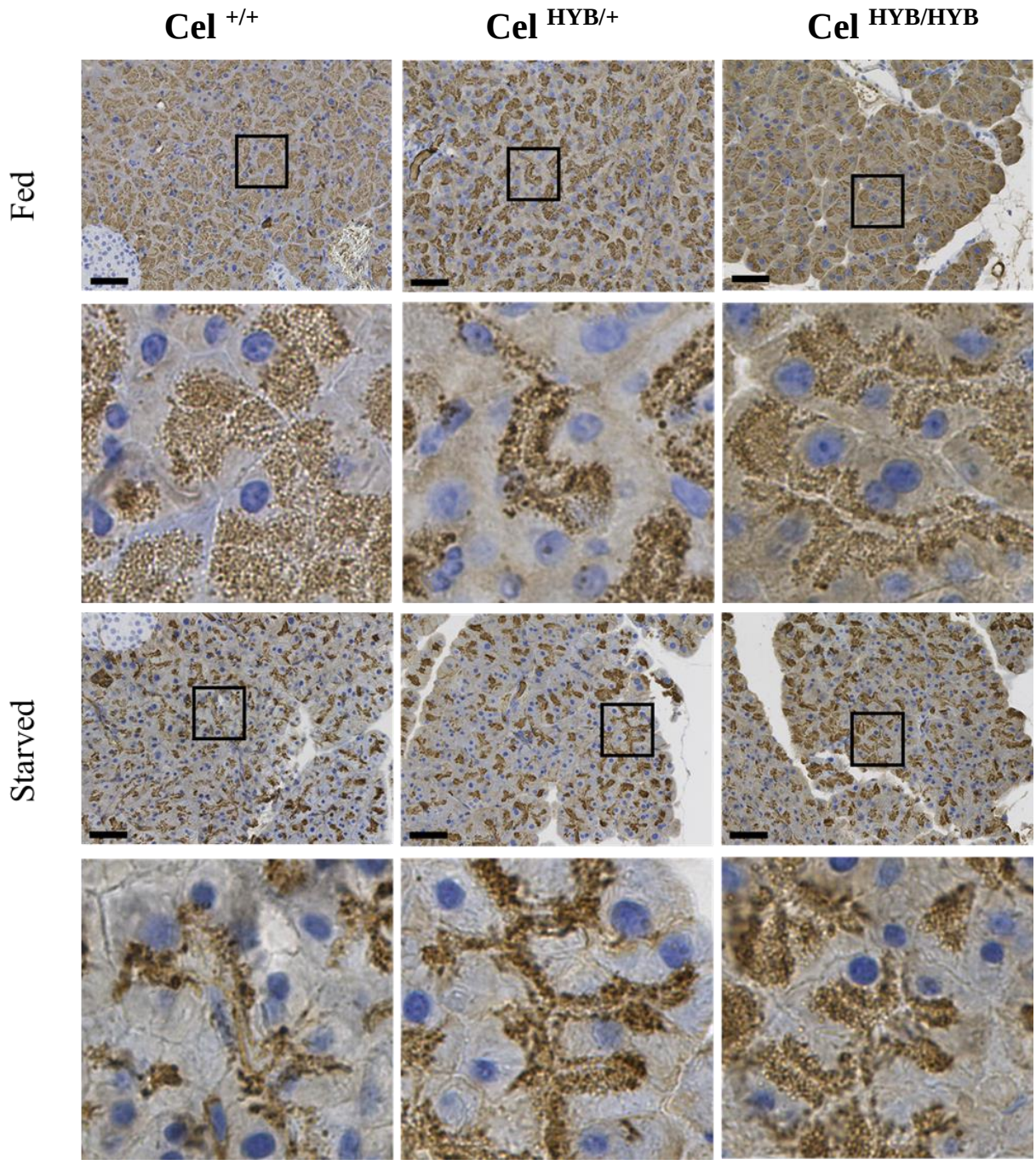

Figure 5.7. Immunohistochemistry for Cel in pancreatic tissue from 6-month-old Cel-HYB mice. Pancreas sections from fed and starved control ($Cel^{+/+}$), heterozygous ($Cel^{+/HYB}$) and homozygous ($Cel^{HYB/HYB}$) mice. *Scale bar: 50 µm.*

When staining for LC3B, we had to start by optimizing the protocol since we had no experience with IHC and the anti-LC3B antibody. For this, we used a pancreatic section from a fed 12-month-old $Cel^{HYB/HYB}$ mouse, hoping that this could serve as a positive control. Indeed, as shown in Figure 5.8, LC3B was expressed in the acinar cells and areas of positive staining was observed throughout the exocrine part of the pancreatic section.

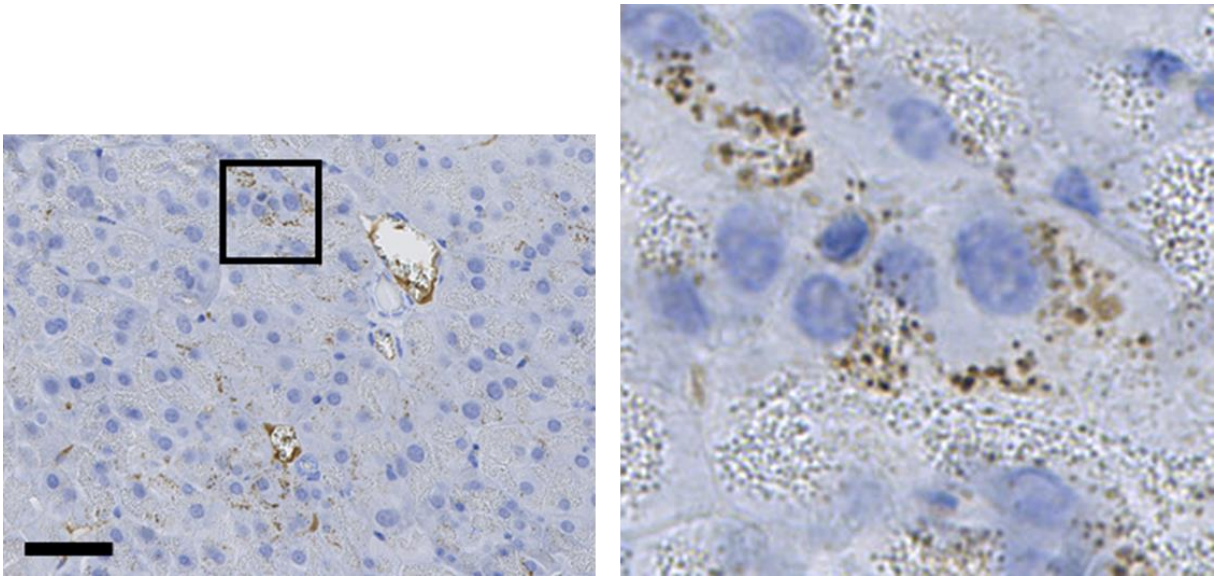

Figure 5.8 Immunohistochemistry for LC3B - a positive control. Pancreas section from a fed $Cel^{HYB/HYB}$ mouse aged 12 months was stained for LC3B and shows multifocal LC3B positive tissue. Positive staining was observed as brown signals. *Scale bar: 50 µm.*

Next, this protocol was used for staining pancreatic sections from fed and starved heterozygous and homozygous 6-month-old Cel-HYB mice, and a control mouse. In the pancreatic section from the fed control mouse the entire section was negative, except for 2 cells, while in the fed heterozygous and homozygous mice there were multiple areas with positive staining (Figure 5.9), although far less than for the 12-month-old mouse. It was not detected any positive LC3B staining in the pancreas of starved mice.

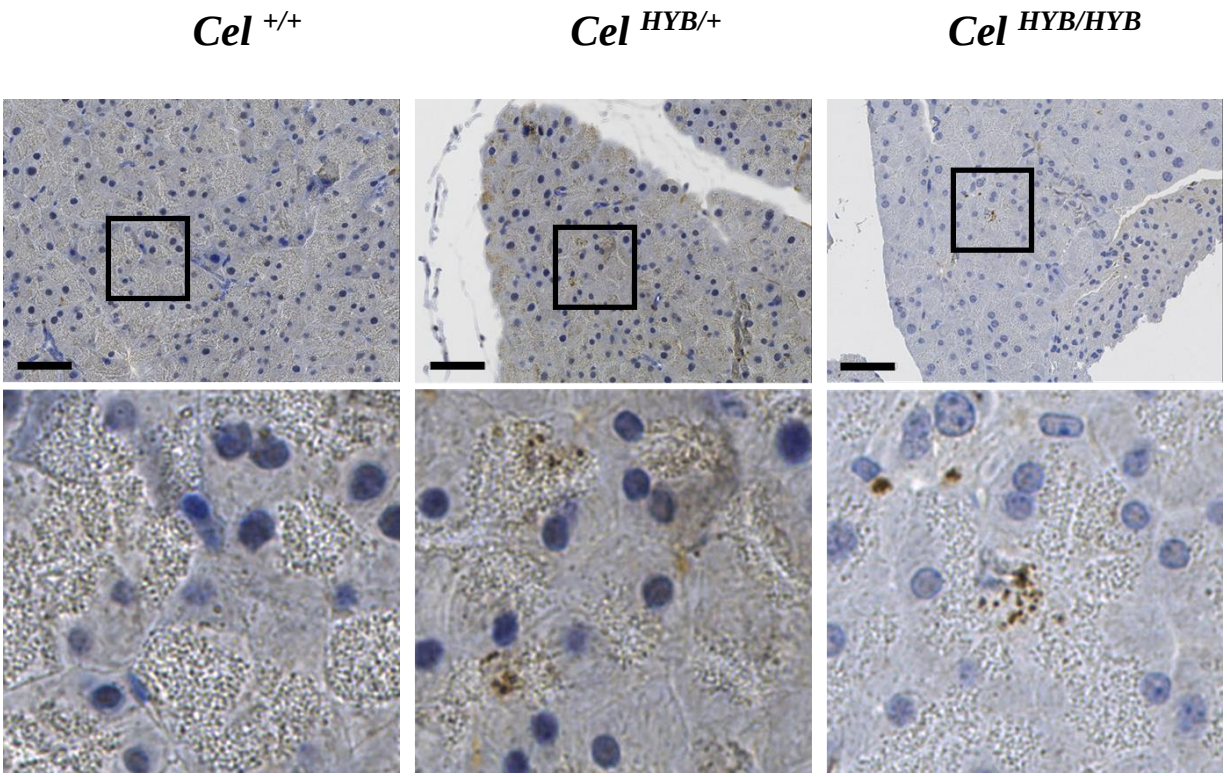

Figure 5.9 Immunohistochemistry for LC3B in pancreatic tissue from 6-month-old Cel-HYB mice. Pancreas sections from fed control ($Cel^{+/+}$), heterozygous ($Cel^{+/HYB}$) and homozygous ($Cel^{HYB/HYB}$) mice. Positive staining was observed as brown signals. *Scale bar: 50 µm.*

5.3 Identification of potential binding partners of CEL-HYB

To search for potential binding partners of CEL-HYB and the wildtype protein, co-immunoprecipitations (co-IP) were performed followed by mass spectrometry and proteomics analysis.

5.3.1 Co-IP of V5-tagged CEL protein variants

Co-IP was performed on cell lysate fractions of HEK293 cells transiently transfected with plasmids expressing CEL-WT, CEL-HYB or CEL-TRUNC. EV was used as a negative control. The co-IP procedure was performed using magnetic beads and a tag-directed anti-V5 antibody (section 4.9.3). For the pilot experiment, the antibody-antigen complex was eluted from the beads and analyzed by SDS-PAGE coomassie staining and western blotting before subjected to mass spectrometry (section 4.9.4 and 4.9.5 respectively). This was done to make sure that the method had worked properly. Thus, we should be able to detect our CEL protein variants in sufficient amounts, and also to see other bands on the Coomassie gel, that might indicate protein binding partners.

The three CEL variants were detected on both the Coomassie-stained gel and on the western blot (Figure 5.10). Bands for CEL-WT were detected between 100 kDa and 120 kDa, CEL-HYB at ~ 65 kDa and CEL-TRUNC at ~ 60 kDa. Additional bands observed for all four lanes, including EV, represented background noise. The strong bands observed at about 150 kDa were most likely IgG bands of the anti-V5 antibody released from the magnetic beads together with CEL proteins.

Taken together, these results confirmed that the CEL variants were found at sufficient levels in the immunoprecipitate. Next, the co-IP was repeated, and four technical replicates were performed and subjected to mass spectrometry.

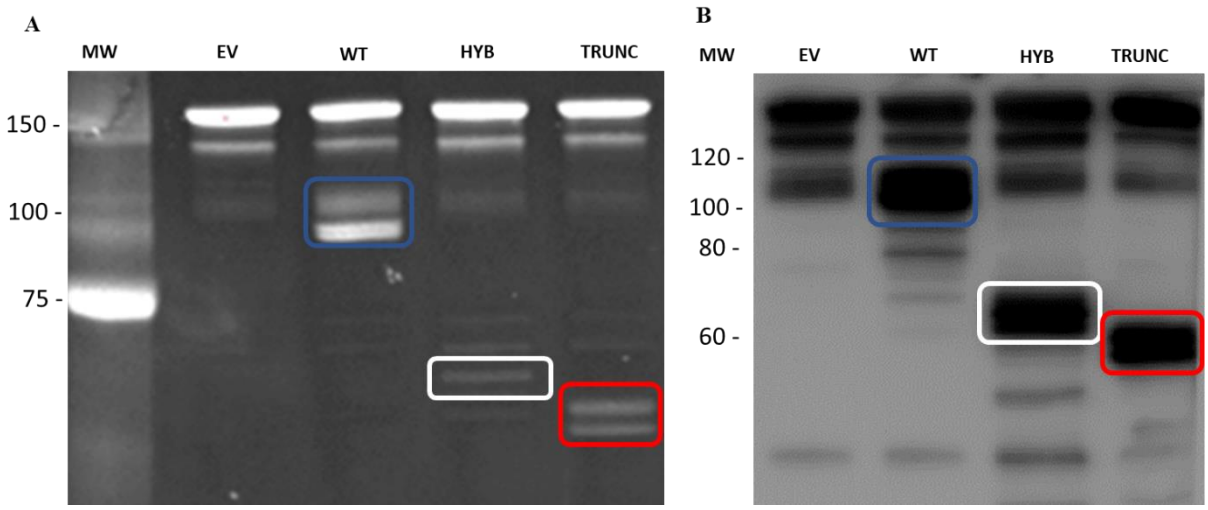

Fig. 5.10 Confirmation of co-IP. HEK293 cells transiently transfected with EV or plasmids expressing CEL-WT, CEL-HYB or CEL-TRUNC were subjected to co-immunoprecipitation. The eluates were analyzed by SDS-PAGE, Coomassie staining **(A)** and western blotting **(B)**. Bands representing the CEL-WT (blue box), CEL-HYB (white box) and CEL-TRUNC proteins (red box) were seen on both the gel and the immunoblot.

5.3.2 Liquid Chromatography-Electrospray Ionization-Mass Spectrometry (LC-ESI-MS)

To identify possible protein binding partners, raw data from LC-ESI-MS was analyzed and visualized using different software. The percentage of overlap between the four replicates from the co-IP experiment was analyzed and visualized by Venn diagram (Figure 5.11). Here, proteins with peptide spectrum matches (PSMs) of 50 or less were excluded. For the CEL-WT, CEL-HYB and CEL-TRUNC replicates, the overlap of all four replicates was above 90%. For the negative control EV, the overlap was 83%. This implies good overlap between replicates, and further analysis could be performed.

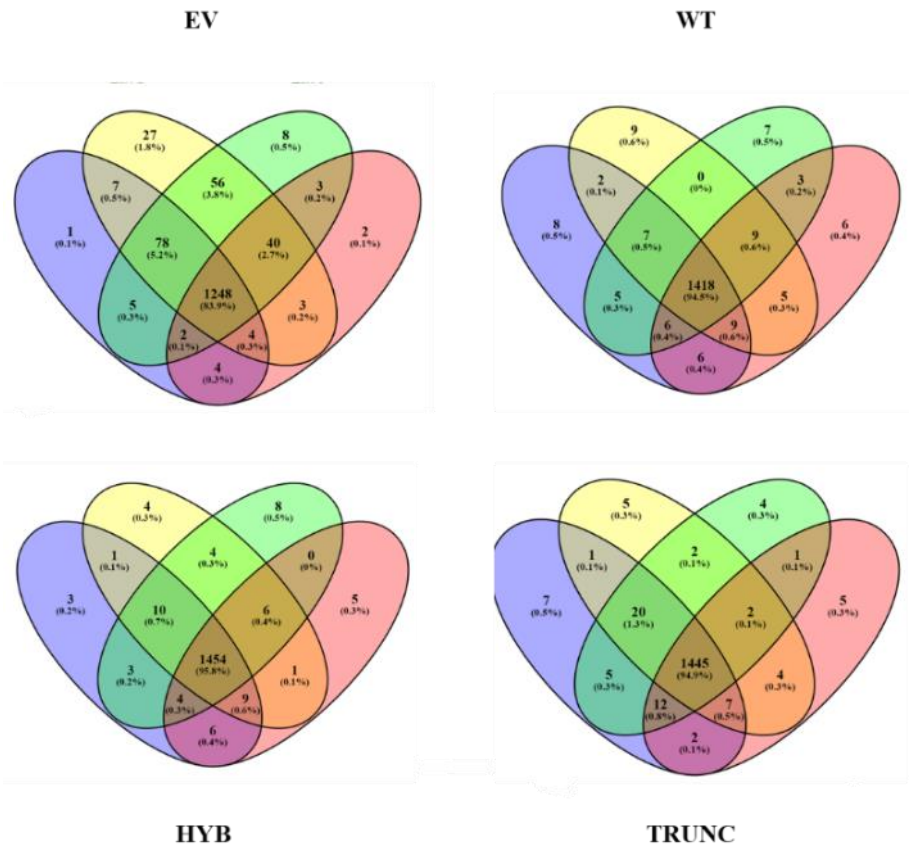

Figure 5.11: Protein overlap between the replicates within each CEL variant sample by Venn's diagram. Comparison of overlap between the replicates within each sample. Visualized in Venny 2.1. *Oliveros, J.C: (2007-2015) Venny.*

Then, to filter the data and further compare the proteome profile of the immunoprecipitants from the different CEL-variants and EV, normalized values were analyzed with the Perseus software. After filtering, we were left with 2960 proteins (section 4.10.3). These proteins were normalized by Z-score, then analyzed and visualized by hierarchical clustering and heat mapping (section 4.10.3) as shown in Figure 5.12. We found that the CEL-WT and EV replicates clustered together. In contrast, CEL-HYB and CEL-TRUNC showed a mixed cluster, suggesting more similar binding partners.

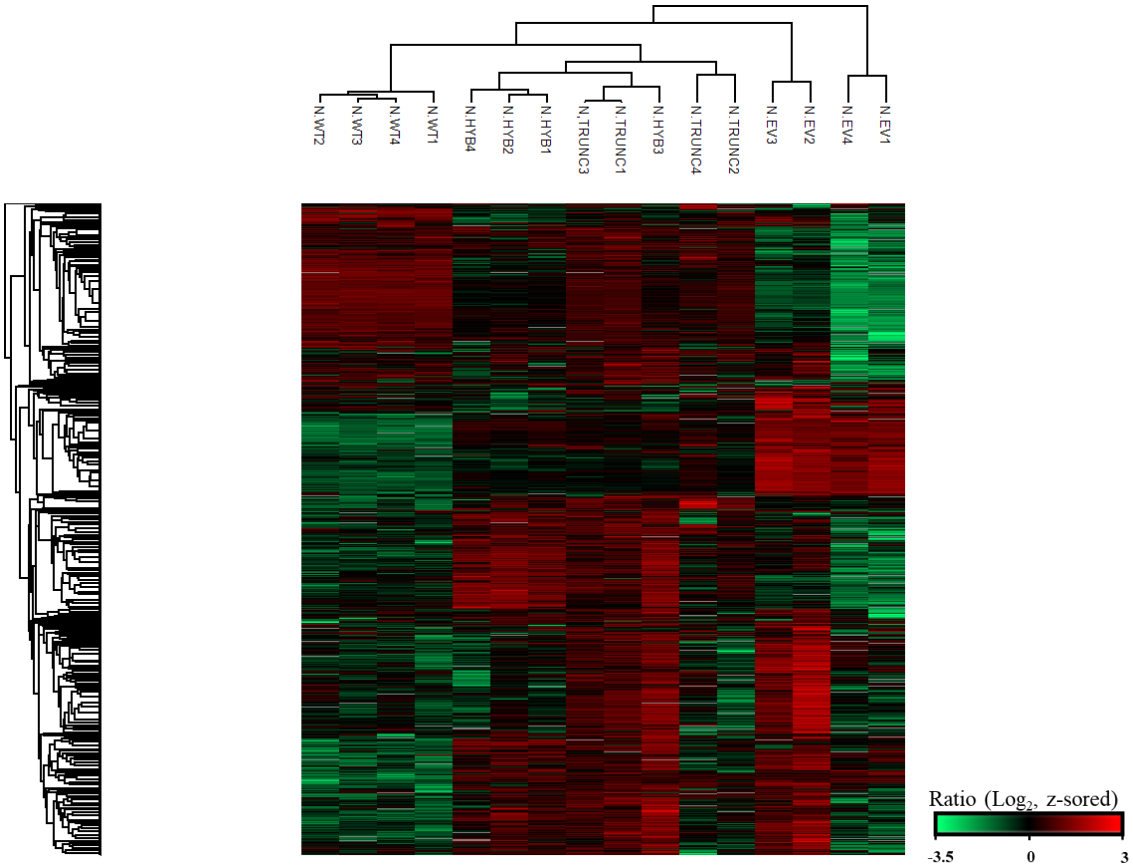

Figure 5.12: Hierarchical clustering and heat map. Hierarchical clustering of normalized values from four replicates of the variants CEL-WT, CEL-HYB, CEL-TRUNC and the negative control EV. Proteins with high and low abundance are shown in red and green, respectively.

5.3.3 Statistical analysis

To find protein binding partners that were significantly different between variants, unpaired t-test was performed. In addition, z-score was used to calculate fold change (FC) significance. The p-value was set to 0.05 or less and FC significance score to 0.01 or less. Here, we decided to compare the proteins bound to CEL-HYB and CEL-WT to EV. We found 155 and 229 significantly different proteins when comparing CEL-HYB to EV and CEL-WT to EV, respectively. These proteins are listed in Supplementary Table 1.

5.3.4 Enrichment analysis and interaction networks

After the statistical analysis, we wanted to see if any of the protein hits could be linked by known protein-protein interaction (PPI) networks. By using the STRING database and ClusterONE analysis, we found several statistically significant clusters of proteins (Supplementary Table 2). Of these, we found one particularly interesting cluster for each of our two comparisons, as both clusters were related to protein folding, however, the clusters included different proteins (Figure 5.13). When comparing CEL-HYB and EV, we found one

downregulated and 8 upregulated proteins (Figure 5.13 A), whereas CEL-WT compared to EV showed 6 downregulated proteins (Figure 5.13 B).

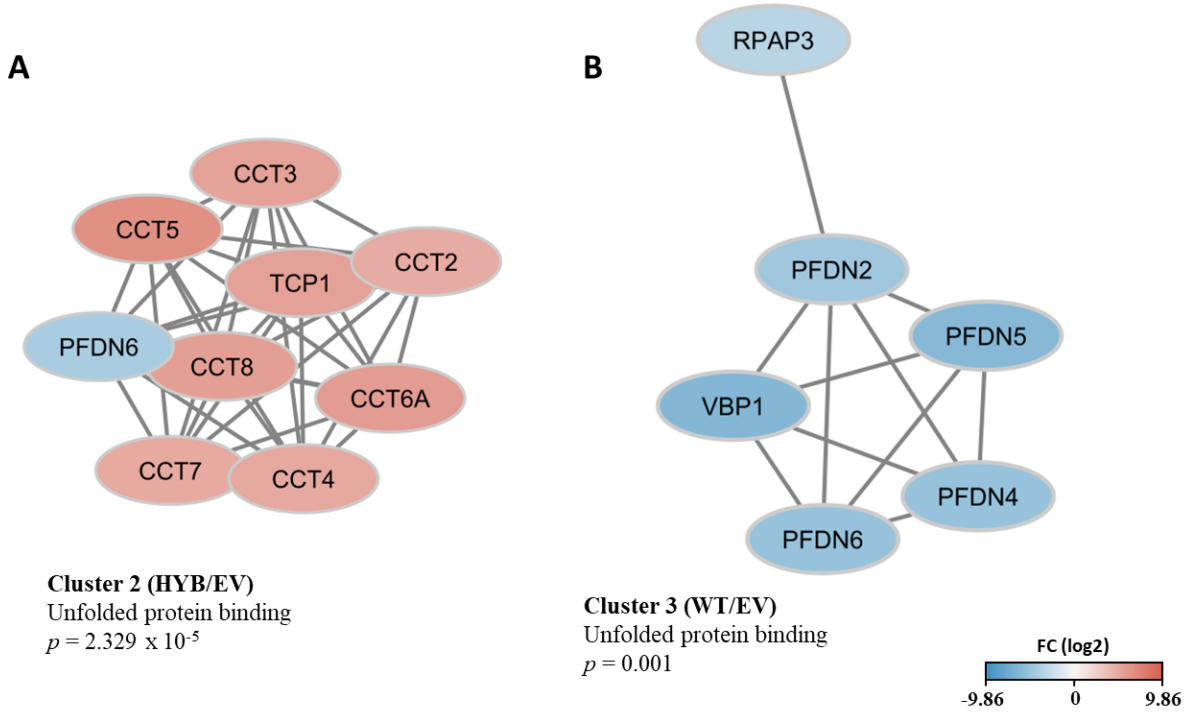

Figure 5.13 Protein-protein interactions networks. Clusters with significant cohesiveness and related to protein folding detected for CEL-HYB **(A)** and CEL-WT **(B)**. Networks from the STRING database were visualized and analyzed in Cytoscape and ClusterONE, respectively, with *p*-value of a one-sided Mann-Whitney U test. The protein nodes are coloured according to their $\log_2$ fold change, i.e., blue indicates reduced abundance and red increased abundance in the HYB/WT group, compared to EV.

6 Discussion

In 2015, *CEL-HYB* was identified by our research group as a novel chronic pancreatitis risk gene, being overrepresented by five-fold in cases compared to healthy controls (63). Functional studies performed in the paper revealed that CEL-HYB was less secreted than normal CEL protein, had reduced enzyme activity, accumulated inside the cell, and induced autophagy in HEK293 cells (63). It is now believed that CEL-HYB belongs to the misfolding-dependent pathway of genetic risk in chronic pancreatitis (78). Changes in amino acid sequence of the protein cause misfolding, leading to ER stress, which may induce inflammatory signaling, and if sustained, this may lead to apoptosis (65, 66). The disease mechanism of CEL-HYB still remains largely unknown. In this thesis, we therefore aimed to learn more about the cellular fate of CEL-HYB and to search for potential protein binding partners.

6.1 The cellular fate of CEL-HYB

6.1.1 Intracellular aggregation and reduced secretion of CEL-HYB

To study the cellular fate of CEL-HYB, we first used HEK293 cells and performed transient transfection followed by cellular fractionation and western blotting. We found that compared to CEL-WT, both CEL-HYB and CEL-TRUNC were significantly less secreted from the cells ($p < 0.0001$), had significantly lower protein levels in the lysate ($p < 0.0001$) and were present in much higher amounts in the insoluble pellet fraction (Figure 5.2). Although the increased amount of CEL-HYB in the pellet was not statistically significant compared to CEL-WT ($p=0.1927$), it showed a trend that coincided with previous findings (63, 65). Thus, the initial results of this thesis confirmed previous findings in HEK293 cells and strengthen the hypothesis that CEL-HYB is a misfolded protein that tend to aggregate inside the cell. Interestingly, CEL-HYB and CEL-TRUNC have similar properties, possibly due to both having a short C-terminal.

Overall, these results encouraged further studies on intracellular degradation pathways: how does the cell handle the expression of aggregating CEL-HYB proteins?

6.1.2 CEL-HYB and autophagy

6.1.2.1 CEL-HYB and autophagy in HeLa-cells

In the discovery paper of CEL-HYB, autophagy was suggested as a potential degradation pathway for the pathogenic protein (63). Western blot analysis showed increased levels of the autophagy marker LC3B in HEK293 cells (human embryonic kidney cells) expressing CEL-

HYB compared to CEL-WT. Here, to investigate the process further, we wanted to test whether CEL-HYB and LC3B were colocalizing in the cell. LC3B is the most studied LC3 isoform when studying autophagy (79). Our hypothesis was that if CEL-HYB induced autophagy, we would expect to find the aggregating protein enclosed by autophagosomes including the membrane-bound LC3B-II protein (80). We performed transfection of *CEL* variants, followed by immunostaining and confocal imaging, but unfortunately, the experiment failed because of technical issues. Due to lack of time, the experiment could not be repeated. However, prior to the co-immunostaining, the immunostaining protocol was optimized for CEL and LC3B alone. From these results we found that CEL proteins are mainly located in the Golgi apparatus and dispersed throughout the ER (Figure 5.3 A). For CEL-HYB and CEL-TRUNC, we observed larger dot-like structures in the periphery of ER, compared to cells expressing CEL-WT (Figure 5.3.B). These large dot-like structures could in fact be autophagosomes, surrounding CEL proteins. Other explanations for these structures may be secretory vesicles, however, since CEL-WT is secreted more than CEL-HYB it would be expected fewer secretory vesicles present in cells expressing CEL-HYB. In the starved cells, we could see that the same large dot-like structures were found in cells expressing CEL-HYB and CEL-TRUNC, but also in cells expressing CEL-WT, meaning that both starvation and CEL-HYB may induce the same intracellular pathways, resulting in the same immunostaining pattern.

We then stained for the autophagy marker LC3B and observed large dot-like structures peri-nuclear in the cells. It was not a clear difference between the patterns of LC3B in these cells transfected with different *CEL*-variants. We also starved the cells because starvation is a major inducer of autophagy (63). The same patterns were seen for the starved cells as for the fed cells. Since the cells were not co-stained with CEL, we could not decide if the LC3B-positive cells had also been successfully transfected with *CEL*. The intensity of the staining could not be compared between cells since the laser intensity on the confocal microscope was not set at the same level for all cells. This was due to differences in signal between each cell, and much signal would either get lost or be over-exposed if the laser intensity was standardized. Compared to cells transfected with EV, we observed more positive cells transfected with *CEL-WT, CEL-HYB* or *CEL-TRUNC*. One possible reason for positive LC3B staining in EV cells is that the cells get stressed by the transfection itself, which in turn increases autophagy. Starved cells transfected with EV also had more positive staining than fed EV cells, suggesting that starvation induces autophagy.

6.1.2.2 CEL-HYB and autophagy in pancreatic tissue

To analyze autophagy in the pancreatic tissue, we stained for the autophagy marker LC3B. Interestingly, in our mouse model, we detected positive LC3B staining in pancreas sections from Cel-HYB mice, but not control mice (Figure 5.8 and 5.9). For the 12-month-old positive-control mouse ($Cel^{HYB/HYB}$) large areas of the pancreatic tissue were LC3B positive (Figure 5.8). For the 6-month-old Cel-HYB heterozygous and homozygous mice, only a couple of areas had positive LC3B staining (Figure 5.9). This may indicate that the level of autophagy increases with age. Our findings of LC3B in Cel-HYB mouse pancreas concur with data from a recently published study by Mao et. al from China (81). The Chinese research group also generated a new Cel-HYB mouse model; however, their mice express the human protein from exon 2, while our mouse model express the mouse protein with only exon 11 changed to the human version. Mao et. al concludes that expression of the human CEL-HYB protein in Cel-HYB mice induces activation of autophagy in a time-dependent manner. When we stained pancreatic tissue from starved mice, it was not possible to conclude if there were any positive LC3B staining, due to high background. Unfortunately, there was not enough time to repeat this staining.

A source of error when staining for LC3B is the primary antibody, since this detects both LC3B-I (the cytosolic form) and LC3B-II (the membrane-bound form), although the antibody has strongest affinity to LC3B-II (82). Only LC3B-II is bound to the autophagosome membrane. It has been shown in ATG9 (autophagy-related gene 9) knock-out cells and ATG7 (autophagy-related gene 7) knock-out mice that LC3B-I can form puncta with the ubiquitin-binding autophagy receptor p62 and accumulate when autophagy is impaired (83). Another problem is that despite positive LC3B-II staining, and instead of the autophagosome being involved in autophagy, the autophagosomes may actually be involved in non-autophagic processes like endocytosis and phagocytosis (84).

In addition to LC3B, pancreas sections from fed and fasted Cel-HYB mice were analyzed for the presence of Cel protein by IHC. We observed a different Cel protein expression pattern in heterozygous and homozygous Cel-HYB mice, compared to control mice. While the normal mouse Cel protein was being dispersed throughout the apical part of the acinar cells in controls, Cel-HYB was aligned on the inside of the cell membrane, forming tubular-like patterns in large areas of the pancreatic section (Figure 5.7). This finding suggests aggregation of Cel-HYB inside the acinar cells. The tubular pattern was stronger in homozygous than in heterozygous Cel-HYB mice. In the starved mice, we could see signs of the same tubular Cel pattern also for the control mice. For the starved heterozygous and homozygous mice, a stronger tubular pattern

was observed than for controls, which could indicate aggregation of Cel-HYB protein. When starving the mice, digestive enzymes are not secreted from pancreatic acinar cells (20), but waiting to be secreted along the apical cell membrane, this may be why we see similar pattern in the starved control as well.

6.1.2.3 The autophagic flux

One of the difficulties regarding interpretation of LC3B in our cell and mouse experiments, is the autophagic flux (measure of autophagic degradation activity). Detecting LC3B levels does not necessarily correlate to a high or low autophagic flux. In the article from Fjeld et. al (63), this was tested by adding bafilomycin to the transfected HEK293 cells, to block autophagosomes from fusing with lysosomes. LC3B levels were higher when adding bafilomycin, meaning that CEL-HYB most likely does not lead to obstruction in the autophagic pathway (63). If, however, the levels were high both without and when adding bafilomycin, it could indicate obstruction of the fusing of autophagosome and lysosome, and congestion of autophagosomes (85, 86). Increased levels of LC3B in cells expressing CEL-HYB compared to those cells expressing CEL-WT is then likely due to increased autophagic flux.

Furthermore, another challenge with measuring LC3 is that after the autophagosome fuses with the lysosome, some of the LC3B-II leaves the autophagolysosome, and gets turned back into cytosolic LC3B-I, while some of the LC3B-II is digested inside the autophagolysosome. This decreases the total level of LC3B-II in the cell (87). Lower amounts of LC3B-II would then be a result of increased turnover, rather than low autophagic flux. A possible way of measuring autophagic flux in the mouse pancreas using IHC is to use transgenic LC3 mice where the LC3B protein has been fused with GFP and RFP. When both GFP and RFP is expressed autophagosomes are detected as yellow puncta, while autolysosomes are detected as red puncta, since GFP is pH-sensitive and gets degraded in the acidic lysosome (88). One of the problems, however, is that there may be a slow and gradual transition from autophagosome to autolysosome, and from acidic to basic pH, which makes the method less sensitive (88).

6.2 Protein binding partners of CEL-HYB

To better understand the cellular fate of CEL in health and disease, we set out to search for CEL protein binding partners. Based on current knowledge, the only reported CEL protein binding partner is the ER chaperone GRP94 (89). In that study, it was suggested that a multimeric complex including GRP94 may be important for secretion of CEL, in addition to preventing premature aggregation of CEL proteins.

There are several approaches available for detecting protein-protein interactions. Since we wanted to express CEL in mammalian cells, because of the extensive post-translational modifications (PTMs) of CEL, the two-hybrid system (90) and glutathione-S-transferase (GST) -pulldown system (91) were not an option. Other methods are tandem affinity purification tagging (92) and co-immunoprecipitation (93). For this study, we chose to transiently express CEL variants in HEK293 cells followed by co-immunoprecipitation and proteomic analysis.

6.2.1 Identifying possible protein binding partners for CEL-HYB and CEL-WT

After mass spectrometry, the identified proteins were filtered in Perseus software and statistically significant proteins were listed (Supplementary Table 1). There were 155 and 229 statistically significant possible binding partners for CEL-HYB and CEL-WT, respectively. The proteins were analyzed in STRING, a database of known and predicted protein-protein interactions (PPIs). The PPIs from the STRING database were imported to CytoScape for visualization of the protein's fold change, and significant protein cohesiveness, using ClusterOne (Figure 5.13). The most significant clusters for the PPIs were then further analyzed in STRING, looking at gene ontology (GO) and KEGG pathways. Even if stringent criteria in STRING were set, false positives could occur. Our analysis shows us that we have three significant protein clusters for CEL-HYB and four for CEL-WT (Supplementary Table 2).

When looking at the significant proteins in cells expressing CEL-HYB compared to EV, 3 significant clusters were found (Supplementary Table 2). The most significant and biggest cluster was spliceosome proteins. The second significant cluster (p 2.329×10^{-5}) was very interesting, some of its biological processes and molecular functions (GO) were positive regulation of establishment of protein localization to telomere (FDR = 9.47×10^{-21}), chaperone mediated protein complex assembly (FDR = 0.0087), protein stabilization (FDR = 3.55×10^{-13}), protein folding (FDR = 1.88×10^{-15}), and unfolded protein binding (FDR = 2.3×10^{-17}). In this cluster, 8 out of the 9 proteins were upregulated in cells expressing CEL-HYB compared to EV, and highly relevant to the protein CEL-HYB, since it is thought to aggregate and belong to the misfolding-dependent pathway. The reasons for this cluster being upregulated could be true upregulation, either as binding partners of CEL-HYB or unspecific binding to the antibody, or down-regulated or low degree of unspecific binding in EV. The only protein in this cluster, also found in cells expressing CEL-WT was prefoldin subunit 6 (PFDN6), being downregulated in both samples.

We found four significant clusters for CEL-WT (Supplementary Table 2), all of which were downregulated in CEL-WT, compared to EV. The most significant and biggest cluster was

related to spliceosome and RNA degradation, like in the CEL-HYB sample. The second significant cluster was related to mRNA. None of them were interesting to us since it is not expected that these proteins are related to the disease mechanism of CEL-HYB. The third significant cluster (*p* 0.001), however, was very interesting, with the biological process and molecular function (GO) being protein folding (FDR = 1.25×10^{-5}) and unfolded protein binding (FDR = 4.89×10^{-5}) , respectively. All 6 proteins in the cluster were down-regulated in CEL-WT compared to EV. In theory, there should be no proteins in the EV samples, since only CEL should bind to the antibody in co-IP. However, unspecific bindings occur, and since there is no CEL to compete for the antibody seats in EV samples, more background can bind in EV samples than in samples with CEL. Since binding affinity affects the results, it can be challenging to interpret the result as down- or upregulation. One reason for the discovery of the first cluster can be high amounts of spliceosome proteins in cells, increasing the chance of unspecific binding to antibodies. Alternatively, one or more of the proteins in the cluster might have a high affinity to the antibody, pulling down the rest of the cluster. Another reason for unspecific binding could be incubating the bead-antibody-antigen complex for too long since specific bindings reach equilibrium faster than unspecific bindings.

6.3 Choice of methods and study challenges

6.3.1 Choice of cell line

HEK293 cells are embryonic kidney cells, while HeLa cells originate from a cervical adenocarcinoma. Both cell lines have been immortalized. We chose to transfect HEK293 and HeLa cells because they are human cells, enabling them to produce our protein with correct post-translational modifications (PTMs) and folding. However, since they are not a pancreatic acinar cell line, the exact machinery necessary for correct PTM may deviate from acinar cells. Particularly O-glycosylation is important because the VNTR region of CEL is heavily O-glycosylated, and this protects the protein against degradation. Correct folding is also very important, since misfolded or unfolded CEL-HYB is believed to be a misfolding-dependent pathway of genetic risk in chronic pancreatitis (65). HEK293 and HeLa cells are secretory cells, this trait is important for a digestive enzyme. However, they do not have the proper physiological conditions for regulated secretion (95), the secretory pathway for CEL therefore varies from acinar cells. The cells also need to be transfected with *CEL* and produce a large number of recombinant proteins, which may affect the folding and PTMs of the protein and the metabolism of the cell.

There are no commercially available human pancreatic acinar cell lines available, only rodent acinar cell lines, like rat AR42J and mouse 266-6. These cells produce digestive enzymes and may provide a more suitable environment to study chronic pancreatitis. The downside of using them is that they are cancer cell lines and may show different characteristics than healthy acinar cells, in addition to not being human, which may affect the PTM outcome. Our group has previously transfected mouse 266-6 acinar cells, where transfection and immunoblotting showed to be challenging, and treatment with dexamethasone was needed to ensure proper acinar cell phenotype. HEK293 and HeLa cells, on the other hand, are easy to transfect, grow rapidly and adapt well to cultivation (96). We chose HeLa cells instead of HEK293 for IF because of their morphology, having larger cytoplasm, making it easier to observe CEL and LC3B in the microscope.

6.3.2 Transient transfection

We chose to transiently transfect the cells, meaning they do not integrate the transgenic plasmid into their genome and therefore the *CEL* gene will not be replicated. CEL is therefore only expressed for a certain period of time, usually several days. One of the benefits of transient transfection compared to stable transfection is the experiment can be done just 8 to 96 hours post-transfection.

6.3.3 The use of V5-tagged plasmids

To detect and purify our CEL protein variants, a V5 epitope tag was fused to the recombinant CEL protein. V5-tags are small peptide tags of 14 amino acids and can be used in methods like immunofluorescence, immunoprecipitation, and western blotting. One of the advantages of using V5 tags are easy detection of the protein by using an anti-V5 antibody. On the other hand, the tag may affect structure and function of the protein (97).

6.3.4 Starvation of cells

When starving HeLa cells, we tried different starvation protocols. In the first protocol (presented in this thesis), we used DMEM with pyruvate, but no glucose or fetal bovine serum (FBS) for 3 hours. We then repeated this protocol but starved the cells for 2 hours only to reduce the high mortality rates. Nutrient deprivation triggers pro-survival signals like autophagy and the unfolded protein response. However, if there is a sustained lack of nutrients, it promotes cell death. We did, however, not observe much difference in mortality rates (not quantified). In the second protocol, we used DMEM with pyruvate, but no glucose, FBS or amino acids for 2 hours. In the third protocol, we used DMEM with pyruvate and glucose, but no amino acids or

FBS for 2 hours. Similar results with regard to mortality were seen for all three protocols (not quantified).

6.3.5 Pros and cons of co-IP

Co-IP is a widely applied technique to isolate protein complexes from a solution by using antibodies. One of the benefits of this technique is that it captures both bait (CEL) and prey proteins (binding partners) in their native conformation, which is important since protein bindings and interactions hugely depend on the proteins' conformation. The interaction networks also form in non-denaturing, and almost physiological conditions. However, low affinity bindings or transient interaction partners are unlikely to be detected, and the result cannot confirm if the target proteins bind directly to the bait protein or via another protein. Since the co-IP was performed in HEK293 cells, protein binding partners expressed in pancreatic acinar cells, but not in HEK293 cells, will not be detected. Also, proteins expressed in HEK293 which are not produced in acinar cells may interfere with CELs' PPI networks. In theory, interactions detected could occur after cell lysis, since subcellular compartments get exposed to one another, and proteins normally not being in physical contact could interact. When transfecting the cells with pcDNA3.1 plasmids expressing *CEL* under the control of a strong promoter (CMV), the cells will overexpress the protein, which may trigger non-physiological interactions.

There are several choices to make before performing a co-IP, e.g., choice of beads (agarose, Sepharose or magnetic), and binding method. In the direct binding method, antibodies are first added to the beads, before adding cell lysate to the pre-formed bead-antibody complex, while in the indirect method, antibodies are first added to cell lysate before adding the beads to the antibody-antigen complex. The kit employed in this study is based on the direct binding method, which is suitable if the target protein is present in higher amount or there is less antibody. We chose to use a co-IP kit protocol with magnetic beads. One of the benefits of using magnetic beads are no need for centrifugation, which potentially can destroy protein-protein interactions. Moreover, it is easy to remove flow-through without losing some of the pellet, it reduces protocol time, and less antibody is needed since all antibodies are available on the outside of the beads, in contrast to other types of beads where some antibodies may be trapped in pores, unavailable for antigen. The beads are coated with either Protein A or Protein G, both of which have strong affinity towards the fragment crystallizable (Fc) region of mouse IgG2 antibodies, making sure it does not interfere with the antibody's binding to antigen in the fragment antigen binding (Fab) region. In this project, we tried three different protocols (two of which are not

presented in this thesis), all of them using magnetic beads. Since all CEL protein variants were V5-tagged, we used an anti-V5 tagged antibody. Another consideration is to use a non-denaturing lysis buffer, like NP40, not to destroy protein-protein interactions during washing.

The results from mass-spec tell us that the co-IP has not been specific enough. There are several reasons for this to occur, e.g., not sufficiently stringent washing. The balance between washing too hard, which means losing protein interactors, and washing too gently, and risk high background due to unspecific bindings, can be difficult. Another reason for high background is using too much antibody (94). Since we did not measure CEL protein concentration in the cell lysate, the antigen-antibody ratio was not calculated, this may have caused higher background noise, meaning unspecific bindings between the antibody and proteins with lower affinity (high K_D) to the antibody, since CEL does not occupy all the antibody binding seats. Ideally the amount of antibody should be titrated to optimal concentration. Other reasons can be proteins with unspecific binding to the beads; however, this is less likely since the lysate was pre-cleared, meaning that proteins binding to the beads were disposed before performing the co-IP. If we suspected this to be a problem, we simply could repeat the pre-clearing.

7 Concluding remarks

The main purpose of this study was to gain more knowledge about the cellular fate and protein binding partners of the pathogenic CEL-HYB protein. Based on our findings, and when compared to the normal CEL protein of control mice, the following conclusions can be drawn:

- We confirm that CEL-HYB has is less secreted and the protein tends to aggregate inside the cell, when expressed in HEK293 cells.
- The Cel protein is accumulating intracellularly along the apical membrane of the pancreatic acinar cells in mice expressing the Cel-HYB protein, suggesting Cel-HYB protein aggregation.
- CEL-HYB and CEL-TRUNC are showing larger dot-like structures in the peripheral ER when expressed in HeLa cells, indicating the presence of autophagosomes.
- The autophagy marker LC3B is detected in the acinar cells of both heterozygous and homozygous Cel-HYB mice, suggesting that Cel-HYB is inducing autophagy at the organ level, in a time-dependent matter.
- Possible CEL-HYB binding partners are identified, including a cluster of 8 proteins that is linked to protein folding.

8 Future perspectives

More research is needed to fully understand the disease mechanism of CEL-HYB. To follow up on the findings presented in this thesis, our group plans to focus on:

Degradation pathways of CEL-HYB

- We will repeat the immunofluorescence experiment for LC3B and CEL in HeLa cells to see if the two proteins colocalize or not.
- Confirm LC3B positive IHC and IF staining as autophagosomes, e.g., using transmission electron microscopy.
- Investigate if CEL-HYB protein aggregation also can be linked to proteasomal degradation, by looking at ubiquitination of CEL-HYB compared to normal CEL.

CEL-HYB binding partners

- Verify some of the possible protein binding partners identified with co-IP and LC-ESI-MS, by co-IP and western blotting, or immunostaining followed by confocal imaging.
- Optimize co-immunoprecipitation protocol to reduce background in mass spectrometry. Further down-stream analysis of proteomic results.

To investigate the disease mechanisms of CEL-HYB even further, one option could be to use our Cel-HYB mouse model and perform laser tissue dissection followed by RNA sequencing/proteomics. In this way, we could compare the RNA/protein expression profiles of the pancreatic exocrine tissue in Cel-HYB and control mice.

9 References

1. Holck P. Bukspyttkjertelen Store medisinske leksikon, snl.no2020 [updated 10.06.2020. Available from: https://sml.snl.no/bukspyttkjertelen.
2. SJ. P. The Exocrine Pancreas. San Rafael (CA): Morgan & Claypool Life Sciences2010.
3. Dolenšek J, Rupnik MS, Stožer A. Structural similarities and differences between the human and the mouse pancreas. Islets. 2015;7(1):e1024405.
4. Talathi SS ZR, Young M. . Anatomy, Abdomen and Pelvis, Pancreas. StatPearls (Internet): StatPearls Publishing, Treasure Island (FL); 2021.
5. Paniccia A, Schulick RD. Chapter 4 - Pancreatic Physiology and Functional Assessment. In: Jarnagin WR, editor. Blumgart's Surgery of the Liver, Biliary Tract and Pancreas, 2-Volume Set (Sixth Edition). Philadelphia: Elsevier; 2017. p. 66-76.e3.
6. Saito K, Iwama N, Takahashi T. Morphometrical analysis on topographical difference in size distribution, number and volume of islets in the human pancreas. Tohoku J Exp Med. 1978;124(2):177-86.
7. Campbell JE, Newgard CB. Mechanisms controlling pancreatic islet cell function in insulin secretion. Nat Rev Mol Cell Biol. 2021;22(2):142-58.
8. Delta Cell Anatomy Ancyclopaedia Britannica Inc [Available from: https://www.britannica.com/science/delta-cell.
9. Turkish A, Husain SZ. 80 - Pancreatic Development. In: Wyllie R, Hyams JS, editors. Pediatric Gastrointestinal and Liver Disease (Fourth Edition). Saint Louis: W.B. Saunders; 2011. p. 878-89.e5.
10. Napolitano T, Silvano S, Vieira A, Balaji S, Garrido-Utrilla A, Friano ME, et al. Role of ghrelin in pancreatic development and function. Diabetes, Obesity and Metabolism. 2018;20(S2):3-10.
11. Da Silva Xavier G. The Cells of the Islets of Langerhans. J Clin Med. 2018;7(3).
12. Britannica TEoE. Islets of Langerhans Encyclopedia Britannica2020 [Available from: https://www.britannica.com/science/islets-of-Langerhans.
13. Longnecker DS. Anatomy and Histology of the Pancreas Pancreapedia: Exocrine Pancreas Knowledge Base2021 [
14. Gondré-Lewis MC, Park JJ, Loh YP. Chapter Two - Cellular Mechanisms for the Biogenesis and Transport of Synaptic and Dense-Core Vesicles. In: Jeon KW, editor. International Review of Cell and Molecular Biology. 299: Academic Press; 2012. p. 27-115.
15. Bergman R.A AAK, Heidger P.M. Atlas of Microscopic Anatomy: Section 10 -Digestive System: Anatomy Atlases. An anatomy digital library; [Available from: http://www.anatomyatlases.org/.
16. Whitcomb DC, Lowe ME. Human Pancreatic Digestive Enzymes. Digestive Diseases and Sciences. 2007;52(1):1-17.
17. Greene KG. Pathology of the Pancreas. In: Reisner HM, editor. Pathology: A Modern Case Study. New York, NY: McGraw-Hill Education; 2015.
18. Marino C R GFS. Pancraetic and salivary glands [2nd:[Available from: https://doctorlib.info/physiology/medical-physiology-molecular/44.html.
19. Anagnostides A, Chadwick VS, Selden AC, Maton PN. Sham feeding and pancreatic secretion. Evidence for direct vagal stimulation of enzyme output. Gastroenterology. 1984;87(1):109-14.
20. Pancreatic Juice 2021 [Dictionary]. Available from: https://www.biologyonline.com/dictionary/pancreatic-juice.
21. Physiologic Exocytosis in Pancreatic Acinar Cells and Pathologic Fusion Underlying Pancreatitis [Internet]. American Pancreatic Association 2020.
22. Williams JA. Regulation of acinar cell function in the pancreas. Curr Opin Gastroenterol. 2010;26(5):478-83.
23. Stene LC RP, Åsvold BO, Bjarkø VV, Sørgjerd EP, Njøstad I, Hopstock LA, Birkeland KI, Gulseth HL. Hvor mange har diabetes i Norge i 2020? Tidsskriftet Den Norske Legeforening. 2020(17).
24. Kaul K. TJM, Ahmad S.I., Kohner E.M., Chibber R. Introduction to Diabetes Mellitus. (eds) ASI, editor. New York, NY.: Springer; 2013.
25. American Diabetes A. Diagnosis and classification of diabetes mellitus. Diabetes Care. 2013;36 Suppl 1(Suppl 1):S67-S74.

26. Herndon J. What is monogenic Diabetes? Healthline: Healthline 2021 [Available from: https://www.healthline.com/health/diabetes/monogenic-diabetes.
27. Lemelman MB, Letourneau L, Greeley SAW. Neonatal Diabetes Mellitus: An Update on Diagnosis and Management. Clin Perinatol. 2018;45(1):41-59.
28. MODY mody.no: Center for Diabetes Research (University of Bergen) and Haukeland University Hospital 2021 [Available from: mody.no/mody.
29. Zhang H, Colclough K, Gloyn AL, Pollin TI. Monogenic diabetes: a gateway to precision medicine in diabetes. J Clin Invest. 2021;131(3).
30. Helseinformatikk N. Akutt betennelse i bukspyttkjertelen 2021 [Available from: https://nhi.no/sykdommer/magetarm/bukspyttkjertel/bukspyttkjertelbetennelse-akutt/.
31. Lankisch PG, Apte M, Banks PA. Acute pancreatitis. The Lancet. 2015;386(9988):85-96.
32. Aune D, Mahamat-Saleh Y, Norat T, Riboli E. Tobacco smoking and the risk of pancreatitis: A systematic review and meta-analysis of prospective studies. Pancreatology. 2019;19(8):1009-22.
33. Lee PJ, Papachristou GI. New insights into acute pancreatitis. Nature Reviews Gastroenterology & Hepatology. 2019;16(8):479-96.
34. Beyer G, Habtezion A, Werner J, Lerch MM, Mayerle J. Chronic pancreatitis. The Lancet. 2020;396(10249):499-512.
35. Helseinformatikk N. Kronisk betennelse i bukspyttkjertelen 2020 [Available from: https://nhi.no/sykdommer/magetarm/bukspyttkjertel/bukspyttkjertelbetennelse-kronisk/.
36. Singh VK, Yadav D, Garg PK. Diagnosis and Management of Chronic Pancreatitis: A Review. JAMA. 2019;322(24):2422-34.
37. Tan M, Schaffalitzky de Muckadell OB, Jørgensen MT. [Hereditary pancreatitis]. Ugeskr Laeger. 2020;182(7).
38. Rosendahl J, Bödeker H, Mössner J, Teich N. Hereditary chronic pancreatitis. Orphanet J Rare Dis. 2007;2:1-.
39. PRSS1 gene: MedlinePlus; 2020 [Available from: https://medlineplus.gov/genetics/gene/prss1/#conditions.
40. Helseinformatikk N. Kreft i bukspyttkjertelen 2022 [Available from: https://nhi.no/sykdommer/kreft/magetarm-kreft/bukspyttkjertelkreft/?page=1.
41. Zhao Z, Liu W. Pancreatic Cancer: A Review of Risk Factors, Diagnosis, and Treatment. Technol Cancer Res Treat. 2020;19:1533033820962117-.
42. Vincent A, Herman J, Schulick R, Hruban RH, Goggins M. Pancreatic cancer. The Lancet. 2011;378(9791):607-20.
43. Lidberg U, Nilsson J, Strömberg K, Stenman G, Sahlin P, Enerbäck S, et al. Genomic organization, sequence analysis, and chromosomal localization of the human carboxyl ester lipase (CEL) gene and a CEL-like (CELL) gene. Genomics. 1992;13(3):630-40.
44. Raeder H, Johansson S, Holm PI, Haldorsen IS, Mas E, Sbarra V, et al. Mutations in the CEL VNTR cause a syndrome of diabetes and pancreatic exocrine dysfunction. Nat Genet. 2006;38(1):54-62.
45. Johansson BB, Fjeld K, El Jellas K, Gravdal A, Dalva M, Tjora E, et al. The role of the carboxyl ester lipase (CEL) gene in pancreatic disease. Pancreatology. 2018;18(1):12-9.
46. Vanin EF. Processed pseudogenes. Characteristics and evolution. Biochim Biophys Acta. 1984;782(3):231-41.
47. Madeyski K, Lidberg U, Bjursell G, Nilsson J. Structure and organization of the human carboxyl ester lipase locus. Mamm Genome. 1998;9(4):334-8.
48. Holmes RS, Cox LA. Comparative Structures and Evolution of Vertebrate Carboxyl Ester Lipase (CEL) Genes and Proteins with a Major Role in Reverse Cholesterol Transport. Cholesterol. 2011;2011:781643-.
49. Hui D.Y. H, P.N. Carboxyl ester lipase: structure.function relationship and physiological rolie in lioprotein metabolism and atherosclerosis. Journal of Lipid Research. 2002;43(12):2017-30.
50. Lombardo D, Guy O, Figarella C. Purification and characterization of a carboxyl ester hydrolase from human pancreatic juice. Biochim Biophys Acta. 1978;527(1):142-9.
51. Bläckberg L, Lombardo D, Hernell O, Guy O, Olivecrona T. Bile salt-stimulated lipase in human milk and carboxyl ester hydrolase in pancreatic juice: are they identical enzymes? FEBS Lett. 1981;136(2):284-8.

52. Hui DY, Kissel JA. Sequence identity between human pancreatic cholesterol esterase and bile salt-stimulated milk lipase. FEBS Lett. 1990;276(1-2):131-4.
53. Lombardo D. Bile salt-dependent lipase: its pathophysiological implications. Biochim Biophys Acta. 2001;1533(1):1-28.
54. Rogers S, Wells R, Rechsteiner M. Amino acid sequences common to rapidly degraded proteins: the PEST hypothesis. Science. 1986;234(4774):364-8.
55. Gravdal A, Xiao X, Cnop M, El Jellas K, Johansson S, Njølstad PR, et al. The position of single-base deletions in the VNTR sequence of the carboxyl ester lipase (CEL) gene determines proteotoxicity. J Biol Chem. 2021;296:100661.
56. Loomes KM, Senior HE, West PM, Roberton AM. Functional protective role for mucin glycosylated repetitive domains. Eur J Biochem. 1999;266(1):105-11.
57. Loomes KM, Senior HEJ. Bile salt activation of human cholesterol esterase does not require protein dimerisation. FEBS Letters. 1997;405(3):369-72.
58. Pasqualini E, Caillol N, Valette A, Lloubes R, Verine A, Lombardo D. Phosphorylation of the rat pancreatic bile-salt-dependent lipase by casein kinase II is essential for secretion. Biochem J. 2000;345 Pt 1(Pt 1):121-8.
59. El Jellas K, Dušátková P, Haldorsen IS, Molnes J, Tjora E, Johansson BB, et al. Two new mutations in the CEL gene causing diabetes and hereditary pancreatitis: How to correctly identify MODY8 cases. J Clin Endocrinol Metab. 2021.
60. Pellegrini S, Pipitone GB, Cospito A, Manenti F, Poggi G, Lombardo MT, et al. Generation of β Cells from iPSC of a MODY8 Patient with a Novel Mutation in the Carboxyl Ester Lipase (CEL) Gene. The Journal of Clinical Endocrinology & Metabolism. 2021;106(5):e2322-e33.
61. Xiao X, Jones G, Sevilla WA, Stolz DB, Magee KE, Haughney M, et al. A Carboxyl Ester Lipase (CEL) Mutant Causes Chronic Pancreatitis by Forming Intracellular Aggregates That Activate Apoptosis*. Journal of Biological Chemistry. 2016;291(44):23224-36.
62. Kahraman S, Dirice E, Basile G, Diegisser D, Alam J, Johansson BB, et al. Abnormal exocrine–endocrine cell cross-talk promotes β-cell dysfunction and loss in MODY8. Nature Metabolism. 2022;4(1):76-89.
63. Fjeld K, Weiss FU, Lasher D, Rosendahl J, Chen J-M, Johansson BB, et al. A recombined allele of the lipase gene CEL and its pseudogene CELP confers susceptibility to chronic pancreatitis. Nature genetics. 2015;47(5):518-22.
64. Zou WB, Boulling A, Masamune A, Issarapu P, Masson E, Wu H, et al. No Association Between CEL-HYB Hybrid Allele and Chronic Pancreatitis in Asian Populations. Gastroenterology. 2016;150(7):1558-60.e5.
65. Tjora E, Gravdal A, Engjom T, Cnop M, Johansson BB, Dimcevski GG, et al. Protein misfolding in combination with other risk factors in CEL-HYB1-mediated chronic pancreatitis. Eur J Gastroenterol Hepatol. 2021;33(6):839-43.
66. Cassidy BM, Zino S, Fjeld K, Molven A, Lowe ME, Xiao X. Single nucleotide polymorphisms in CEL-HYB1 increase risk for chronic pancreatitis through proteotoxic misfolding. Hum Mutat. 2020;41(11):1967-78.
67. Martinez E, Silvy F, Fina F, Bartoli M, Krahn M, Barlesi F, et al. Rs488087 single nucleotide polymorphism as predictive risk factor for pancreatic cancers. Oncotarget. 2015;6(37):39855-64.
68. Martinez E, Crenon I, Silvy F, Del Grande J, Mougel A, Barea D, et al. Expression of truncated bile salt-dependent lipase variant in pancreatic pre-neoplastic lesions. Oncotarget. 2017;8(1):536-51.
69. Dalva M, El Jellas K, Steine SJ, Johansson BB, Ringdal M, Torsvik J, et al. Copy number variants and VNTR length polymorphisms of the carboxyl-ester lipase (CEL) gene as risk factors in pancreatic cancer. Pancreatology. 2017;17(1):83-8.
70. Liebl MP, Hoppe T. It's all about talking: two-way communication between proteasomal and lysosomal degradation pathways via ubiquitin. Am J Physiol Cell Physiol. 2016;311(2):C166-C78.
71. Marshall RS, Vierstra RD. Dynamic Regulation of the 26S Proteasome: From Synthesis to Degradation. Frontiers in Molecular Biosciences. 2019;6.
72. Moulis M, Vindis C. Methods for Measuring Autophagy in Mice. Cells. 2017;6(2).
73. Gubas A, Dikic I. A guide to the regulation of selective autophagy receptors. The FEBS Journal. 2022;289(1):75-89.

74. Neset L, Takayidza G, Berven FS, Hernandez-Valladares M. Comparing Efficiency of Lysis Buffer Solutions and Sample Preparation Methods for Liquid Chromatography–Mass Spectrometry Analysis of Human Cells and Plasma. Molecules. 2022;27(11):3390.
75. Johansson BB, Torsvik J, Bjørkhaug L, Vesterhus M, Ragvin A, Tjora E, et al. Diabetes and pancreatic exocrine dysfunction due to mutations in the carboxyl ester lipase gene-maturity onset diabetes of the young (CEL-MODY): a protein misfolding disease. J Biol Chem. 2011;286(40):34593-605.
76. Torsvik J, Johansson BB, Dalva M, Marie M, Fjeld K, Johansson S, et al. Endocytosis of secreted carboxyl ester lipase in a syndrome of diabetes and pancreatic exocrine dysfunction. J Biol Chem. 2014;289(42):29097-111.
77. Molven A, Fjeld K, Lowe ME. Lipase Genetic Variants in Chronic Pancreatitis: When the End Is Wrong, All's Not Well. Gastroenterology. 2016;150(7):1515-8.
78. Sahin-Tóth M. Genetic risk in chronic pancreatitis: the misfolding-dependent pathway. Curr Opin Gastroenterol. 2017;33(5):390-5.
79. Mareninova OA, Jia W, Gretler SR, Holthaus CL, Thomas DDH, Pimienta M, et al. Transgenic expression of GFP-LC3 perturbs autophagy in exocrine pancreas and acute pancreatitis responses in mice. Autophagy. 2020;16(11):2084-97.
80. Kabeya Y, Mizushima N, Ueno T, Yamamoto A, Kirisako T, Noda T, et al. LC3, a mammalian homologue of yeast Apg8p, is localized in autophagosome membranes after processing. EMBO J. 2000;19(21):5720-8.
81. Mao X-T, Zou W-B, Cao Y, Wang Y-C, Deng S-J, Cooper DN, et al. The CEL-HYB1 Hybrid Allele Promotes Digestive Enzyme Misfolding and Pancreatitis in Mice. Cell Mol Gastroenterol Hepatol. 2022;14(1):55-74.
82. LC3B (D11 XP Rabbit mAb #3868: Cell Signaling Technology; [Available from: https://www.cellsignal.com/products/primary-antibodies/lc3b-d11-xp-rabbit-mab/3868.
83. Runwal G, Stamatakou E, Siddiqi FH, Puri C, Zhu Y, Rubinsztein DC. LC3-positive structures are prominent in autophagy-deficient cells. Scientific Reports. 2019;9(1):10147.
84. Galluzzi L, Green DR. Autophagy-Independent Functions of the Autophagy Machinery. Cell. 2019;177(7):1682-99.
85. Barth S, Glick D, Macleod KF. Autophagy: assays and artifacts. The Journal of pathology. 2010;221(2):117-24.
86. Yoshii SR, Mizushima N. Monitoring and Measuring Autophagy. Int J Mol Sci. 2017;18(9):1865.
87. Mizushima N, Yoshimori T. How to interpret LC3 immunoblotting. Autophagy. 2007;3(6):542-5.
88. Klionsky DJ, Abdel-Aziz AK, Abdelfatah S, Abdellatif M, Abdoli A, Abel S, et al. Guidelines for the use and interpretation of assays for monitoring autophagy (4th edition)(1). Autophagy. 2021;17(1):1-382.
89. Bruneau N LD. Chaperone Function of a Grp 94-related Protein for Folding and Transport of the Pancreatic Bile Salt-dependent Lipase. Journal of Biological Chemistry. 1995;270(22):13524-33.
90. Brückner A, Polge C, Lentze N, Auerbach D, Schlattner U. Yeast two-hybrid, a powerful tool for systems biology. Int J Mol Sci. 2009;10(6):2763-88.
91. Fields S, Song O-k. A novel genetic system to detect protein–protein interactions. Nature. 1989;340(6230):245-6.
92. Puig O, Caspary F, Rigaut G, Rutz B, Bouveret E, Bragado-Nilsson E, et al. The tandem affinity purification (TAP) method: a general procedure of protein complex purification. Methods. 2001;24(3):218-29.
93. Lin J-S, Lai E-M. Protein–Protein Interactions: Co-Immunoprecipitation. In: Journet L, Cascales E, editors. Bacterial Protein Secretion Systems: Methods and Protocols. New York, NY: Springer New York; 2017. p. 211-9.
94. Co-immunoprecipitation (Co-IP): ThermoFisher Scientific; [Available from: https://www.thermofisher.com/no/en/home/life-science/protein-biology/protein-biology-learning-center/protein-biology-resource-library/pierce-protein-methods/co-immunoprecipitation-co-ip.html.
95. Tausk FA, Milgram SL, Mains RE, Eipper BA. Expression of a peptide processing enzyme in cultured cells: truncation mutants reveal a routing domain. Mol Endocrinol. 1992;6(12):2185-96.

96. Malm M, Kuo C-C, Barzadd MM, Mebrahtu A, Wistbacka N, Razavi R, et al. Harnessing secretory pathway differences between HEK293 and CHO to rescue production of difficult to express proteins. Metabolic Engineering. 2022;72:171-87.
97. Booth WT, Schlachter CR, Pote S, Ussin N, Mank NJ, Klapper V, et al. Impact of an N-terminal Polyhistidine Tag on Protein Thermal Stability. ACS Omega. 2018;3(1):760-8.

Appendix

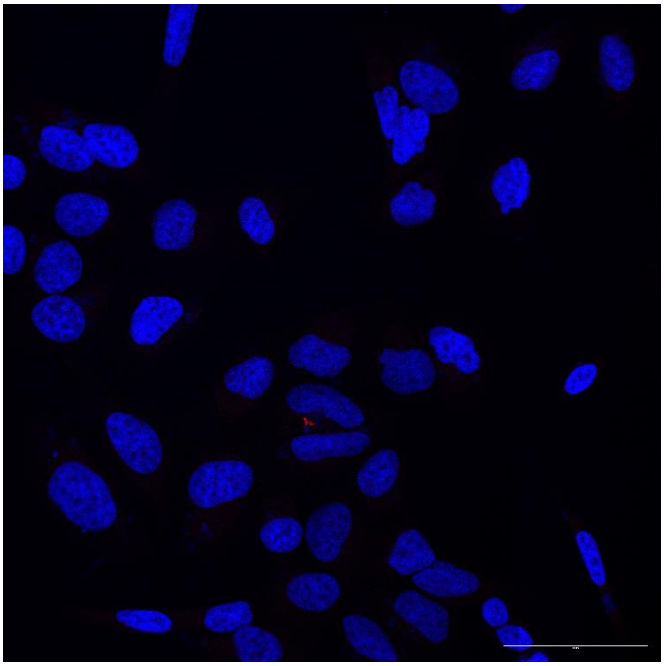

Supplementary Figure 1: Immunofluorescence staining of HeLa cells: negative control. HeLa cells transiently transfected with *CEL-TRUNC* were used as negative control. Here, the primary antibody was replaced by PBS, followed by secondary antibody staining (Alexa-Fluor-488 [green] and Alexa-Fluor-594 [red]). The chromosome counterstain (Hoechst) is shown in blue. The image represents a maximum intensity projection of a z-stack taken through the entire depth of the cell. *Scale bar* 50 µm.

CEL

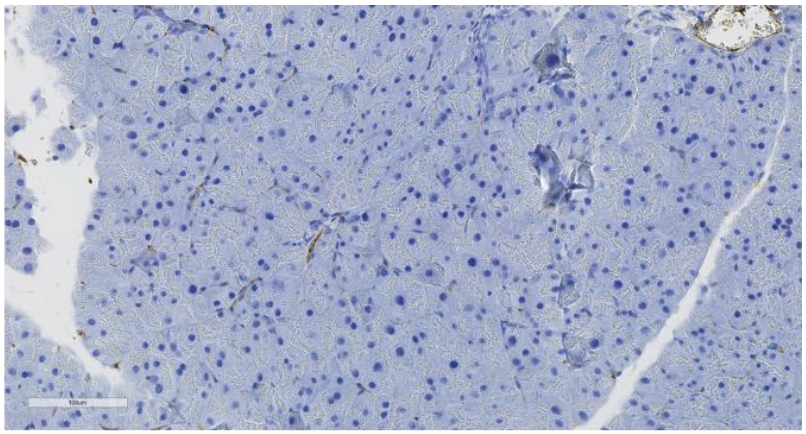

LC3

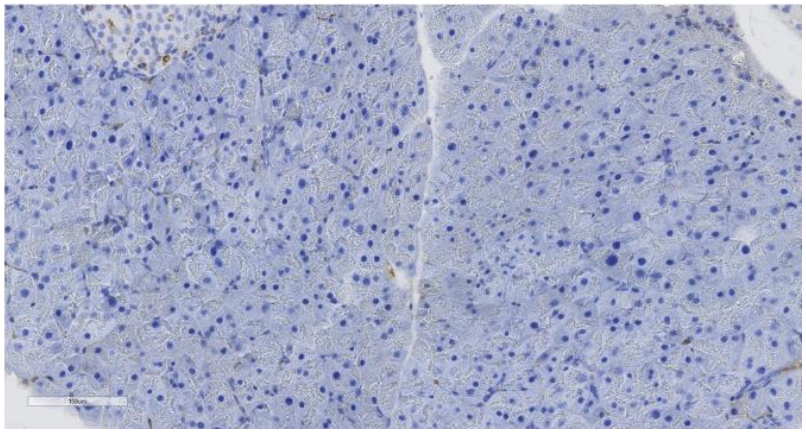

Supplementary Figure 2: Immunohistochemistry of pancreas sections: negative control. IHC of Cel-HYB mouse pancreatic tissue sections where the primary antibody was replaced by PBS, was used as a negative control. *Scale bar* 100 µm.

Supplementary Table 1: After LC-ESI-MS, significantly different proteins were detected between CEL-WT and EV (A), and CEL-HYB and EV (B).

A) After statistical analysis of protein hits from the LC-ESI-MS, the amount of the following 155 proteins were significantly different when comparing CEL-HYB and EV samples. The proteins are listed by their accession numbers.

Column1	Column2	Column3	Column4	Column5	Column6
Q9UQ35	Q2TAY7	P61326-2	Q8N163	Q14517	Q9NZ08
P19835	Q96DI7	Q9UPP1	O00422	Q9BZQ6	Q9NRC1-6
P10809	Q9HCS7	Q9Y5S9	P08069	O14967	Q9BVX2
Q9NYF8	O75152	Q5T200	Q86U44	Q9UEY8	P32780
P48643	Q96FV9	P13995	P49760	Q9BW19	Q9Y5Y5
P49368	Q13769	Q15366-3	Q8NBP0	Q92896	
Q15459	Q15436	Q13356	Q9H1A4	Q96AE7	
Q99832	Q5BKZ1	P07237	Q9BRD0	P62312	
P18583-5	O95816	P27797	Q92522	Q9BZL1	
Q9Y2W1	Q8NAV1	Q9P2E5	Q9BQ52	Q9NSI2	
O60306	O60508	Q12933	Q6I9Y2	Q8N8D1	
P78371	P55081	Q9UHI8	O15212	Q9Y3P9	
Q9H307	Q15428	Q9UKM9	P08236	Q9BQ61	
Q9UKV3	P07910-2	Q9UKJ3	Q9H497	Q9BW66	
P40227	Q5T0W9	O14979	Q9ULR0	Q99741	
P38919	Q96A72	Q92917	Q08170	Q8WXX7	
Q13573	Q14257	Q15287	Q8WXX5	Q16394	
P17987	Q8IWZ8	O95714	Q9H501	O95881	
P50990	Q9BZJ0	P41223	P06280	Q9NXS2	
Q8NI27	P52756	Q92843-2	Q9H444	Q9H6E4	
P50991	Q9BS26	Q9UNP9	O75419	Q92759	
Q9NYU2	Q86W42	Q1ED39	Q99707	Q9Y388	
Q14697-2	Q13162	Q9H4W6-2	Q9Y3C6	Q96IZ7	
Q12874	Q9NW64	Q93063	Q92545	P62310	
Q13123	Q9H0S4	Q9Y4Z0	O95777	Q92626	
Q6PJT7-9	P13667	O75494-3	Q8WUD4	Q9Y2B0	
P30414	Q13427	P29122	P46020	P0DI83	
O43290	Q9HCG8	Q96E39	Q9P013	Q9NVZ3	
Q96T58	Q8N5U6	Q8TAD8	P38935	Q8WV44	
Q9UBS4	Q9NYU1	Q8IXB1	Q99816	Q6P2H3	

B) After statistical analysis of protein hits from the LC-ESI-MS, the amount of the following 229 proteins were significantly different when comparing CEL-WT and EV samples. The proteins are listed by their accession numbers.

Column1	Column2	Column3	Column4	Column5	Column6	Column7	Column8
O15027-5	P30414	Q5T0W9	A91:A120	Q9H4W6-2	Q9ULR0	Q9H7D7	P62310
O75643	P06748	Q96A72	Q9UPP1	O00566	Q9UHV9	P15104	O60870
Q6P2Q9	O43290	Q8IWZ8	Q9Y5S9	Q96NC0	Q8WXX5	Q96QE5	O43719
Q9UQ35	Q96T58	Q9BZJ0	P61962	Q9Y4Z0	Q969Z0	Q9Y2F9	Q8NFQ8
P19835	Q9Y2R4	O95487	Q5T200	Q99848	O60828	P62312	P04637
O75533	Q2TAY7	Q12872	Q15366-3	Q14247	P62314	P62306	Q9Y2B0
Q8NEY1-2	Q96HS1	Q96T37	Q96N67	Q8TAD8	Q9H501	Q9BZL1	Q9NP72
Q15029	Q9Y2W2	P26368	Q13356	O94855	Q13395	Q9Y2S7	Q53S58
Q15393	Q9ULD9	P52756	O95486	Q9NQ55	Q9Y3B4	Q9NQP4	P35813
Q13435	Q96DI7	Q9H6K5	Q14232	Q53H96	Q68D10	Q9NSI2	Q9UMZ2
Q9NYF8	P53992	P68400	Q15427	Q8N163	Q8IWF2	P51153	Q8WV44
O43143	O15014	P09661	Q8IX12	Q2M1P5	Q9H6T3	Q15696	Q7Z2Z1
Q15459	Q14145	Q86W42	P78362-2	O00422	Q9H444	P62304	Q15418-4
P18583-5	Q9HCS7	Q13144	Q16630-2	P67870	O75419	Q9HCE5	Q9UL15
O15042	Q8IWX8	P05198	Q15007	Q9Y3C1	Q9Y3C6	Q8N5L8	Q6P2H3
Q9Y2W1	O75152	Q9NW64	Q9BWJ5	Q9BYG3	Q96EV2	Q9BQ61	P62308
O60306	Q96FV9	P61964	Q8NHQ9	Q86U44	O95777	Q8N954	Q9UK45
Q9H307	Q15437	Q9H0S4	Q9UKM9	P49760	Q9H7B2	Q9BW66	O75323
Q9UKV3	Q9UBB9	Q92769	Q96ME7	Q00059	Q8WUD4	Q99741	Q13557
P38919	Q13769	O43809	Q7Z7F0	O43447	Q9P013	Q9UJW0	
Q9P2R6	Q8N684	Q13427	Q9UKJ3	Q7RTV0	Q9P275	Q8WXX7	
P98175-5	Q15436	P62318	Q92917	Q9BRD0	P63167	Q9BX10	
Q13573	Q9Y5B6	P19784	P14678	Q92522	Q99816	Q9UIV1	
Q15637-5	Q69YN4	P05387	Q15287	Q96DF8	Q99471	Q9UJ70	
Q8NI27	Q5BKZ1	Q9HCG8	O95714	Q49A26	P61758	Q9H3N1	
P55735	Q8NAV1	O60231	P41223	Q92620	Q9Y6A4	Q9Y2G8	
Q12874	O60508	Q86VM9	Q92843-2	Q9BQ52	Q9Y3B9	Q8IVT5	
Q96I25	P55081	P08579	P62316	Q8N5P1	Q03701	P30419	
Q13123	Q15428	Q8N5U6	Q9UNP9	Q6I9Y2	Q9NZJ4	Q96IZ7	
Q6PJT7-9	P07910-2	Q8NFW8	Q1ED39	O15212	Q04917	Q9BRR8	

Supplementary Table 2. Significant clusters of the PPI networks of significant different CEL-HYB (A) and CEL-WT (B) proteins compared to EV. Clusters with significant cohesiveness, their biological process and the *p*-value of a one-sided Mann-Whitney U test.

A)

Cluster 1. RNA binding. $p = 0.000$
Cluster 2. Unfolded protein binding. $p = 2.329 \times 10^{-5}$
Cluster 3. RNA binding. $p = 0.002$

B)

Cluster 1. RNA splicing. $p = 0.000$
Cluster 2. RNA processing. $p = 9.10 \times 10^{-4}$
Cluster 3. Protein folding. $p = 0.001$
Cluster 4. RNA binding. $p = 0.002$